

SOLAR ENERGY RELATED APPLICATIONS, EDUCATION, AND BUILDING
RETROFITS

By

Yunhua Ding

A THESIS

Submitted to
Michigan State University
in partial fulfillment of the requirements
for the degree of

Chemical Engineering – Master of Science

2015

ABSTRACT

SOLAR ENERGY RELATED APPLICATIONS, EDUCATION, AND BUILDING RETROFITS

By

Yunhua Ding

Solar energy technologies have been well development for a wide range of applications. However, research on solar photovoltaics is still being conducted to improve performance and lower installation costs. For example, the power generation potential is not only determined by the intensity or location of solar radiation, but also related to the incident angle of the light. Chapter one explores the effect of angle-dependent characteristic on overall power output for different fixed orientations and configurations by hourly modeling, and the results show substantial improvements are possible.

Michigan State University (MSU) has been promoting building retrofits combining renewable energy, and the Students Planning Advanced Retrofit Technology Applications (SPARTA) is a group that helps MSU address energy initiatives on campus. Chapter two summarizes the overall successes of building retrofit projects including solar rooftop, LED lighting, and window film conducted by the SPARTA group.

The last chapter describes the development of paintable luminescent solar concentrator modules for renewable energy education. The activity is designed for middle school students to understand how energy is generated from solar energy in an inexpensive alternative, which also generates both excitement in solar energy and motivates students to become creative participants in the energy problems.

ACKNOWLEDGMENTS

I would like to thank to my advisor Dr. Richard Lunt for mentoring my research studies and overseeing SPARTA's projects as well as my coadvisor Dr. Andre Benard who has helped on many projects. I also acknowledge Dr. Rebecca Anthony, Andrew Grossman, Joe Hagerty, students in the SPARTA group, Stu Neils, Dan Francis, and other people working at Infrastructure Planning and Facilities (IPF) for their dedication and contributions to SPARTA's projects. Lastly, thanks to all my supportive families and friends who have helped me succeed in life.

TABLE OF CONTENTS

LIST OF TABLES	vi
LIST OF FIGURES.....	vii
KEY TO ABBREVIATIONS.....	vii
OVERVIEW	1
CHAPTER 1 Impact of Photovoltaic Angular Dependency on Overall Power Output	3
1.1 Introduction.....	4
1.2 Solar Cell Background.....	5
1.3 Methods and Calculations	8
1.4 Experiment	11
1.5 Results and Discussion	12
CHAPTER 2 Energy Saving Building Renovation Studies	19
2.1 Introduction	20
2.2 Rooftop Solar Panel Installation	22
2.2.1 Module Design and Operation Background	22
2.2.2 MSU Rooftop Solar Energy Capability Assessment	24
2.2.3 Solar Deployment Analysis Software.....	25
2.2.4 Case Study of Wells Hall.....	27
2.3 Low-e Window Film Energy Saving Study at Kresge Art Center	29
2.3.1 Properties of Window and Window Film.....	29
2.3.2 Cooling System Modeling and Calculation.....	31
2.3.3 Window Film Case Study at Kresge Art Center Results and Discussion.....	33
2.4 LED Lighting Retrofit at Psychology Building	36
2.4.1 Light Fixture Selection	36
2.4.2 Financial Analysis for Psychology Building LED Retrofit.....	38
CHAPTER 3 Outreach Activity – Engaging Students.....	41
3.1 Introduction	42
3.2 Materials and Methods	42
3.2.1 LSC Architecture.....	42
3.2.2 Procedure for Making Paints	44
3.2.3 Educational Kit Assembly	45
3.3 Classroom Activity	46
3.3.1 Class Design	47
3.3.2 Learning Outcome.....	48
SUMMARY AND FUTURE WORK.....	50
APPENDICES	53
APPENDIX I. MSU Rooftop Solar Installation Building List.....	54

APPENDIX II. HelioScope Report of Wells Hall58
BIBLIOGRAPHY65

LIST OF TABLES

Table 1 HAP modeling results.....	34
Table 2 A Comparison of CCT and CRI of F32T8 and CREE UR 2 LED light fixtures.....	37
Table 3 Financial analysis on Psychology Building LED retrofit.....	39
Table 4 Paints recipe for using a single dye	45
Table 5 Paint recipe for using mixed dyes.....	45
Table 6 MSU rooftop solar installation building list.....	54

LIST OF FIGURES

Figure 1 Solar cell schematic figure	5
Figure 2 The concept of fill factor illustrated on JV curve	6
Figure 3 Schematic figure of solar radiation on tilted surface	8
Figure 4 Normalized angle-dependent responsivity for a conventional thin film PV (device A), thin film PV designed for improved angle-dependence (device B), and selected cutoff angle of angle-dependence designed thin film PVs	10
Figure 5 Normalized properties of a representative thin film PV (a) and Si PV (b) versus intensity	12
Figure 6 Normalized yearly power output of Device A at various orientations in (a) Lansing, MI, (b) Phoenix, AZ, and (c) Meru, Kenya. Note that the overall output yearly powers are normalized to the non-tilted (horizontal) configuration.....	14
Figure 7 Normalized yearly power output improvement made by Device B in (a) Lansing, MI, (b) Phoenix, AZ, and (c) Meru, Kenya	15
Figure 8 Normalized yearly power output for idealized responsivities with sharp incident-angle dependent cutoff performance with modules at various tilt angles in Phoenix, AZ	18
Figure 9 (a) Wells Hall elevation map, (b) Wells Hall solar panel layout	28
Figure 10 Heat transfer distributions (a) Before window film application; (b) After window film application	35
Figure 11 Monitored energy consumptions of current fluorescent lights at Psychology Building	38
Figure 12 Sensitivity analysis of LED lighting	40
Figure 14 Luminescent solar concentrator architecture	43
Figure 15 Finished paint solution samples (a) under room light; (b) under UV light.....	44
Figure 16 Education kit assembly.....	46
Figure 17 Students at the painting station	48
Figure 18 (a) Paintings under flashlight on the top of upper right corner; (b) Paintings under flashlight on the top of center; (c) LSC kit assembly with multimeter and motor.	49
Figure 19 Helioscope report capture of Wells Hall	62

KEY TO ABBREIATIONS

AIM: Array impact metric

AM: Air mass

CCT: Correlated color temperature

CRI: Color rendering index

FF: Fill factor

I_{DFH} : METSTAT-modeled diffuse horizontal irradiance (kW/m²)

I_{DFT} : Global tilt irradiance (kW/m²)

I_{DRN} : METSTAT-modeled direct normal irradiance (kW/m²)

I_{DRT} : Direct tilt irradiance (kW/m²)

I_{EH} : Extraterrestrial horizontal irradiance (kW/m²)

I_{GH} : METSTAT-modeled global horizontal irradiance (kW/m²)

I_{GR} : Ground reflected irradiance (kW/m²)

I_{GT} : Global tilted irradiance (kW/m²)

I: Input intensity (kW/m²)

JSC: Photocurrent density (A)

METSTAT: Meteorological-Statistical solar model

MSU: Michigan State University

Q: Yearly power output

R: Responsivity (A/W)

SHGC: Solar heat gain coefficient

SPARTA: Students Planning Advanced Retrofit Technology Applications

VOC: Open-circuit voltage (V)

α : Azimuth angle of the PV module (degrees)

β : Tilt angle of the PV module (degrees)

δ : Improvement of yearly power output

η : Efficiency of a solar cell

θ : Incidence angle of solar ray to PV modules (degrees)

φ : Hourly mean zenith angle of the sun (degrees)

ω : Hourly mean azimuth angle of the sun (degrees)

OVERVIEW

In the spring of 2011, an Energy Transition Plan was initiated at Michigan State University, with the ultimate goal of powering the university with 100% renewable energy [1]. The development of the plan involved the participation of students, faculty, staff, and external advisory groups, and emerged three primary goals from their collaborative efforts: (1) improve the physical environment; (2) invest in sustainable energy research and development; (3) become an educational leader in sustainable energy [1]. Since 2010, the renewable energy portfolio of the university has increased by 8%, and the goal by 2015 is to increase the number to 15% [2].

Students Planning Advanced Retrofit Technology Applications (SPARTA) is a registered student group on campus initiated in response to this Energy Transition Plan. It consists of MSU faculty members and students who are dedicated to promote renewable energy applications using the most effective retrofit technologies. SPARTA has successfully conducted a wide range of projects including research-based studies, engineering analysis, and small-scale field experiments to facilitate MSU to achieve the goal of the Energy Transition Plan. For instance, in chapter one, SPARTA utilizes the resources of campus' labs to make measurements and evaluate the impact of angle-dependent characteristic of solar photovoltaics, which will aid in determining the overall power output from the analysis and modeling on building-integrated photovoltaics retrofit discussed in chapter two. Along with other retrofit options such as LED light and window film, SPARTA has also demonstrated the overall energy savings of a range of buildings in chapter two. Finally, SPARTA's mission and successes are being highlighted by attracting attention to renewable energy applications through educational outreach programs as shown in chapter three. In conclusion, all the chapters reveal SPARTA's effort to make MSU's campus and the world a more sustainable place for the future.

CHAPTER 1

Impact of Photovoltaic Angular Dependency on Overall Power Output

1.1 Introduction

Building Integrated Photovoltaics (BIPVs) have received considerable attention due to their sustainable attributes and functional value [3-5]. A typical BIPV application, for example, is the use of silicon-based or copper indium gallium selenide photovoltaics (PVs) on rooftops and shingles. A significant number of studies have been conducted to identify the optimal tilt angle and orientation to obtain longer periods of near-normal incident illuminated sunlight [6, 7]. However, considering the trajectory of the sun, these deployed solar cells are rarely illuminated at normal incidence. In addition, the high cost of rotational mounting systems and environmental considerations (wind, snow, etc.) have primarily limited practical designs to fixed configurations, and many synergistic BIPV approaches (such as solar shingles) are already necessarily in fixed configurations. Hence, it is critical to design PVs that give stable performance over a range of incident angles.

In comparison to traditional silicon-based PV applications, thin film and organic photovoltaic technologies have increased their market share due to their potential for light weight, flexible, and transparent applications [8]. Importantly, thin film PVs can be designed to have specific angle dependence properties [9-11] with the improvement of external and internal quantum efficiencies [12, 13]. Moreover, window integrated solar cells are gaining attention due to the development of transparent photovoltaics (TPVs) which have exceptional low-cost potential and are enabled by new excitonic materials [14, 15]. In this case, TPVs can be considered for siding, windows, and skylights, which normally have fixed structures [16]. Recently, TPV designs with enhanced angle-dependence were demonstrated, leading to the improvements in responsivity by as much as 50% at particular oblique angles with nearly identical performance at normal

incidence [17-19]; the improvements were achieved by considering and optimizing layer structures for non-normal incidence.

For all of these PV technologies, fixed configuration deployment situations naturally lead to the question: what impact can the designs with minimized angle-dependence have? Here, the overall power output for the TPV designs with different responsivities over varying incidence angle and solar radiation was evaluated to assess the impact of angle-dependent PV efficiency in a range of configurations and locations.

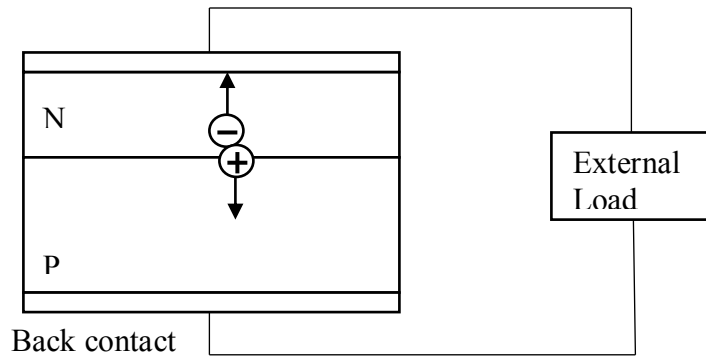


Figure 1 Solar cell schematic figure

1.2 Solar Cell Background

Many solar cells are composed of p-n junctions using semiconductors. The photons from sun light is absorbed, and if the energy exceeds the band gap, electrons will be excited to the conduction band and holes will left behind. The electron-hole pairs can be separated at the p-n junction by the intrinsic electric field such that electrons can move to the external circuit and the holes will penetrate through the p-type material of the p-n junction (Figure 1). The electrons and holes will recombine at the rear contact to complete the circuit.

The quantum efficiency is the ratio of the number of electrons generated to the number of photons absorbed. Each wavelength of light corresponds to different energy, which yields a

unique quantum efficiency at that wavelength. The external quantum efficiency is calculated from the light left after the transmission and reflection of light, and the internal quantum efficiency includes all the photons of light. The internal quantum efficiency is affected by the surface recombination and diffusion length of a solar cell. For high energy wavelength, surface recombination commonly occurs such that quantum efficiency is reduced. For low energy wavelength and low diffusion length, rear surface recombination causes the quantum efficiency to decrease. For the energy below band gap, the quantum efficiency is zero. The overall efficiency of a solar cell is the ratio of the maximum power output from the solar cell to the power of the incident light. To compare across different solar cells, the standard testing condition is AM 1.5, 1 kW/m^2 , and $25 \text{ }^\circ\text{C}$. The efficiency of a module can be different even using the same solar cell because it is related to the packing density of the module. The overall efficiency is essentially determined by short-circuit current (J_{SC}), open-circuit voltage (V_{OC}), and fill factor (FF). The short-circuit current is the current when the voltage across the solar cell is zero, which

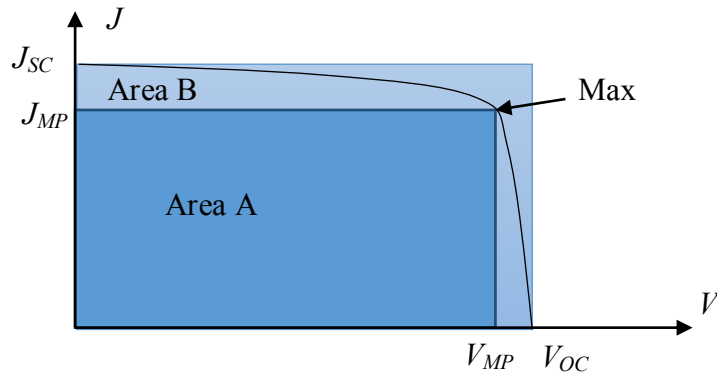


Figure 2 The concept of fill factor illustrated on JV curve

is the largest current a solar cell can generate. It depends on the area of solar cell, the intensity and spectrum of the incident light, the optical properties of solar cell materials, diffusion length, and surface passivation. Therefore, the actual external current output from a solar cell is always lower than the short-circuit current. The open-circuit voltage is the maximum voltage when the

current across the solar cell is zero. The saturation current, which is the current generated in dark environment, affects the open-circuit voltage the most, and it depends on the recombination in the solar cell, or essentially, the carrier concentration in the p-n junction. The fill factor is the ratio of actual maximum power to the product of open-circuit voltage and short-circuit current (Figure 2). On the JV curve, it is the ratio of maximum rectangular area (area A) below the curve to the rectangular area surrounded by open-circuit voltage and short-circuit current (area B). A higher open-circuit voltage usually has a higher fill factor.

The position of the sun changes throughout the day and seasons, so when viewing its location from a fixed location on the Earth, the variations of its radiation can have a significant effects on the amount of sunlight particular locations receive throughout the year. From morning to evening, the sun moves from east to west, and for those geographical regions north of the Tropic of Cancer, the sun appears in the southern sky majority time of the year. Therefore, when it comes to availability of direct solar illumination for higher latitude locations in the northern hemisphere, south facing directions are almost always the best choice to harvest solar energy from – as is the case with the MSU campus.

The azimuth and zenith angles are the most common location measurements used to describe the sun's position as it traces across the earth's surface. The azimuth angle is simply the horizontal angular distance from the north facing direction rotating clockwise. For example, when the sun is positioned in the north, east, south, and west the azimuth angles are 0° , 90° , 180° , and 270° , respectively. The zenith angle is just the complementary angle of the elevation angle, which is, in part, the altitude of the sun measured from the horizon.

The photovoltaic industry has developed a single common standard for evaluating the performance of PV materials, spectrally known as the “American Society for Testing and

Materials (ASTM) G-173-03". The reference spectra, which incorporate both a standard direct normal spectral irradiance and a standard total spectral irradiance as a function of wavelength, represent the terrestrial solar spectral irradiance received at air mass (AM) 1.5. This is measured under a specified atmospheric condition on a standard surface of 37° , tilted toward the equator, facing the sun [20]. The air mass is the actual distance of light travelling through the atmosphere as compared to the direct normal distance defined as: $AM = 1/\cos(\text{zenith angle})$. The increase in AM relates to a larger power reduction of the light due to the absorption by air and dust in the atmosphere at longer travelling distances.

1.3 Methods and Calculations

The Typical meteorological year, version 3 (TMY3) data set contains hourly actual time-series meteorological measurements and modeled solar including solar radiation data for specific locations under typified conditions over 20 years period, and it has been widely used by building designers for modeling renewable energy conversion systems. With the provided azimuth angle, zenith angle, direct normal irradiance and diffuse irradiance, the radiation on a tilted surface can be calculated (Figure 3).

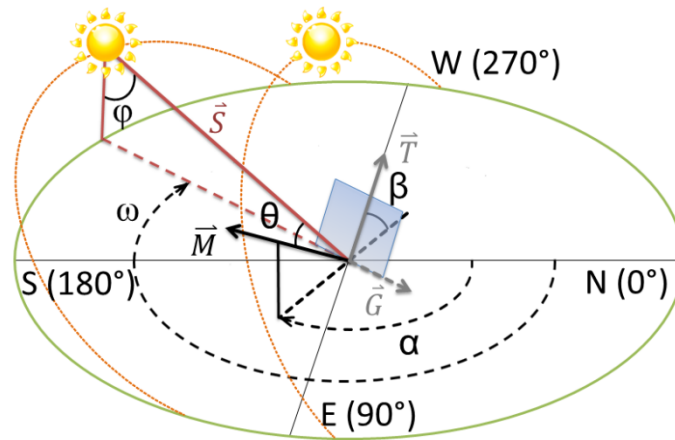


Figure 3 Schematic figure of solar radiation on tilted surface

The calculation follows the separation method described in the Hay model[21]:

$$I_{GT} = I_{DRN} \cdot \cos \theta + I_{DFT} + I_{GR} \quad (\text{Eq. 1})$$

and

$$I_{DFT} = I_{DFH} \left[\frac{(I_{GH} - I_{DFH}) \cos \theta \cos \varphi}{I_{EH}} + \frac{(1 - (I_{GH} - I_{DFH}))(1 + \cos \beta)}{2} \right] \quad (\text{Eq. 2})$$

where I_{DRN} is the direct normal irradiance; I_{DFT} is the diffuse tilted irradiance; I_{GR} is the ground reflected irradiance; I_{GH} is the global horizontal irradiance; I_{GR} is the ground reflected irradiance; I_{DFH} is the diffuse horizontal irradiance; I_{EH} is the extraterrestrial horizontal irradiance; θ is the incident angle of direct solar irradiance with respect to the PV module; φ is the zenith angle of the sun with respect to the horizon; ω is the azimuth angle of the sun with respect to north; β is the tilt angle of the PV module with respect to the horizon; and α is the azimuth angle of the PV module (Figure 3). The solar irradiance is modeled by the Meteorological-Statistical solar method (METSTAT) [22]. Here, I_{GR} can be neglected due to the insignificant impact on I_{GT} comparing to the I_{DT} and I_{DFT} [23]. Then, θ is calculated by

$$\theta = \cos^{-1}(\vec{S} \cdot \vec{M}) \quad (\text{Eq. 3})$$

where $\vec{S} = (\omega, \varphi - 90^\circ, 1)$ is the unit vector of incoming radiation, and \vec{M} is the normal vector of the PV module defined in the left-handed spherical coordinate system $(\alpha, \beta, 1)$, which is calculated from a unit vector within the ground plane, $\vec{G} = (\alpha - 90^\circ, 0^\circ, 1)$, and a second unit vector perpendicular to \vec{G} within the tilted plane, $\vec{T} = (\alpha + 180^\circ, \beta, 1)$, of the PV module as $\vec{M} = \vec{T} \times \vec{G}$.

Hourly instantaneous power output (Q_i) is calculated from the power conversion efficiency of the PV module (η) and the illumination flux (I) by

$$Q_i(\theta, I) = \eta(\theta, I) \cdot I = [FF(\theta, I) \cdot V_{oc}(\theta, I) \cdot R(\theta, I)] \cdot I \quad (\text{Eq. 4})$$

where R is the responsivity calculated from $R(\theta, I) = J_{sc}(\theta, I)/I$; J_{sc} is the short-circuit photocurrent density; V_{oc} is the open-circuit voltage; and FF is the fill factor.

To determine the effect of θ and I , angular dependency and intensity are assumed to be essentially independent so that

$$\eta(\theta, I) = \eta(\theta, I_{ref}) \cdot \eta(\theta_{ref}, I) \quad (\text{Eq. 5})$$

where the reference intensity is 1 mW/mm^2 (1-sun), and the reference incident angle is 0° .

While the impact of angular dependency on FF and V_{oc} is typically negligible[15], the intensity

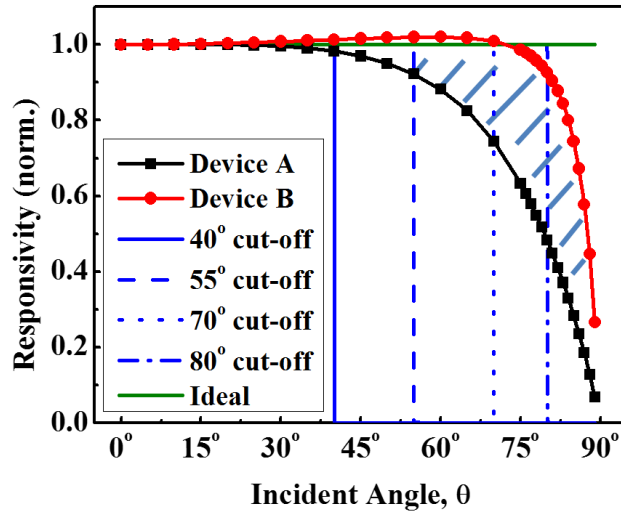


Figure 4 Normalized angle-dependent responsivity for a conventional thin film PV (device A), thin film PV designed for improved angle-dependence (device B), and selected cutoff angle of angle-dependence designed thin film PVs

dependencies of FF , V_{oc} , and R are nonetheless captured in the intensity dependent component of experimentally determined efficiencies. Therefore, the angle dependent component of η is proportional to the angle dependent R at a fixed I [17].

In the simulation of yearly power output, the average value of responsivity (\bar{R}) over $0^\circ - 90^\circ$ incident angle is used for the diffuse irradiance components. Then, the yearly power output (Q) is evaluated for a conventional thin film PV (device A), a thin film PV architecture designed with improved angle dependence (device B) [17], and devices with idealized angle-dependent cutoffs shown in Figure 4 as

$$Q(\theta, I) = \sum_{i=1}^{\tau} [(R(\theta, 1) \cdot I_{DRN,i} + \bar{R} \cdot I_{DFT,i}) \cdot 1 \text{ hr}] \quad (\text{Eq. 6})$$

where τ is the number of hours in one year. The yearly power output for A and B were normalized to the power output of device A at $\beta = 0^\circ$, and the yearly power output for the cutoff devices were normalized to the ideal device response at each tilt. The ideal integrated flux data are typically found to be consistent with monthly and yearly averaged values within 10 – 15% of values reported elsewhere across a range of locations and orientations [24].

1.4 Experiment

The current density versus voltage (JV) characteristics were measured for an archetypal a mono-Si PV (Narec Solar) and a thin film solar cell composed of a chloroaluminiumphthalocyanine (ClAlPc) – C_{60} planar heterojunction[17] under various incident angles and overall light intensities. The former was chosen for its high efficiency and the latter was chosen because of its potential use in transparent PVs for building integrated applications and its use in PVs with high photovoltage approaching the Shockley-Queisser limit [25]. To determine the intensity dependence at normal incidence, a Newport 67005 Arc Lamp with an AM1.5 Filter and a series of neutral density filters (Thorlabs) were used to provide different light intensities, which were corrected by the solar spectrum mismatch factor at each intensity [26]. To characterize the incident angle dependence, the external quantum efficiencies (EQE) of the solar

cells were measured with a lock-in amplifier (Stanford Research System SR830 DSP) and a picoammeter (Keithley 485) at various angles with respect to a fixed monochromatic light source controlled by a substrate rotation stage (Newport). The light source underfilled all devices with a chopped beam at 77 Hz. The EQE was then integrated with the product of the solar flux to give the angle-dependent responsivity.

1.5 Results and Discussion

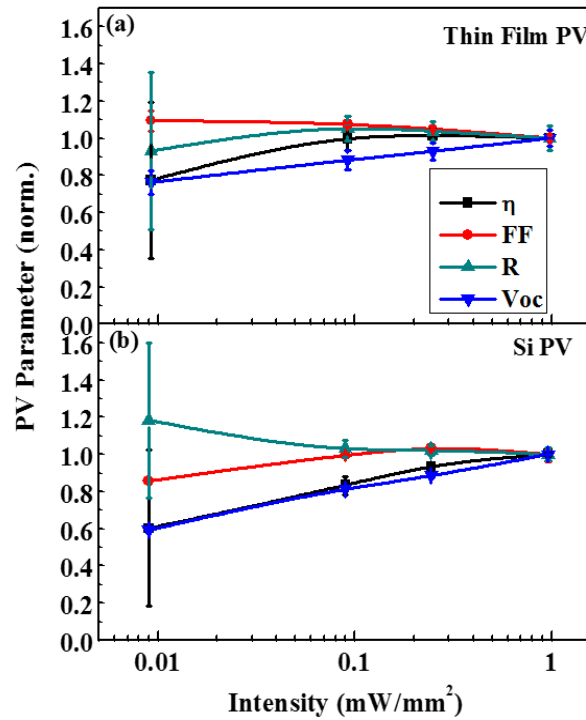


Figure 5 Normalized properties of a representative thin film PV (a) and Si PV (b)

versus intensity

PV performance characteristics of the archetypal thin film PV and mono-Si PVs are normalized to those devices at normal incidence and one sun illumination, and shown in Figure 5 as a function of intensity. Smaller intensity dependence is observed in FF , R , and V_{OC} for the thin film PV compared to the Si PV. For the Si PV, this intensity dependence primarily stems from larger reductions in the V_{OC} . For the thin film PV, the R decreases only slightly with decreasing

intensity, while FF increases slightly. The opposite trend is seen for the Si PV. Consequently, the η for the Si PV shows a logarithmic intensity dependence while the η for the thin film PV is essentially constant across all intensities above 0.1 mW/mm^2 , below which the uncertainties in the measurement begin to dominate. The trend of the η shown in Figure 5 suggests that the thin film PV would perform well throughout the day because sunlight illumination is often above 0.1 mW/mm^2 , and its efficiency is constant in this regime. Since the overall intensity dependence is not significant for the thin film PV, it does not significantly impact the overall power generation.

The output power performances of the two thin film PV device designs with significant variation in the angle dependence (Figure 4) are compared in Figure 6 and Figure 7. Device B, a thin film architecture designed with angle dependence in mind, exhibits limited efficiency roll-off with incidence angle compared to the conventional structure (device A). Figure 6 shows the normalized yearly power output of device A (Q_A) at various PV orientations for Lansing, MI, Phoenix, AZ, and equator represented by Meru, Kenya. The PV orientation covers the full 360° range of azimuth angle with 30° increment and selected tilt angles of 0° (horizontal), 30° , 60° , and 90° (vertical). The overall power output is clearly the same at all orientations when the tilt angle is 0° since the PV is in a horizontal configuration. When the tilt angle (θ) is $> 0^\circ$, a symmetric response appears with a maximum at the south-facing direction ($\alpha = 180^\circ$) for Lansing and Phoenix (Figure 6a and b). This is because the irradiance and incident angle are maximized for the south-facing orientation and are similar for the east-facing and west-facing orientations. The power output is diminished for Lansing and Phoenix when facing north because the sun mostly appears in the southern sky for latitudes above 1.5°N and the photoresponse stems primarily from diffuse irradiance [6]. However, the variation in power output is greater for lower latitude locations due to a greater variation in incident angle. In addition, the optimal tilt angles

which yield the largest overall power output are close to 30° for Lansing and Phoenix, and 0° for Meru, which are consistent with previous reports [6, 23, 27] and closely related to the latitude. As the tilt angle diverges from the optimal tilt angle, the irradiance decreases in all directions, which reduces the overall power output.

The trends are different for tilted devices in Meru (Figure 6 c): the data are asymmetrical and reveal peaks at the east-facing and west-facing directions with a higher value for the west-facing

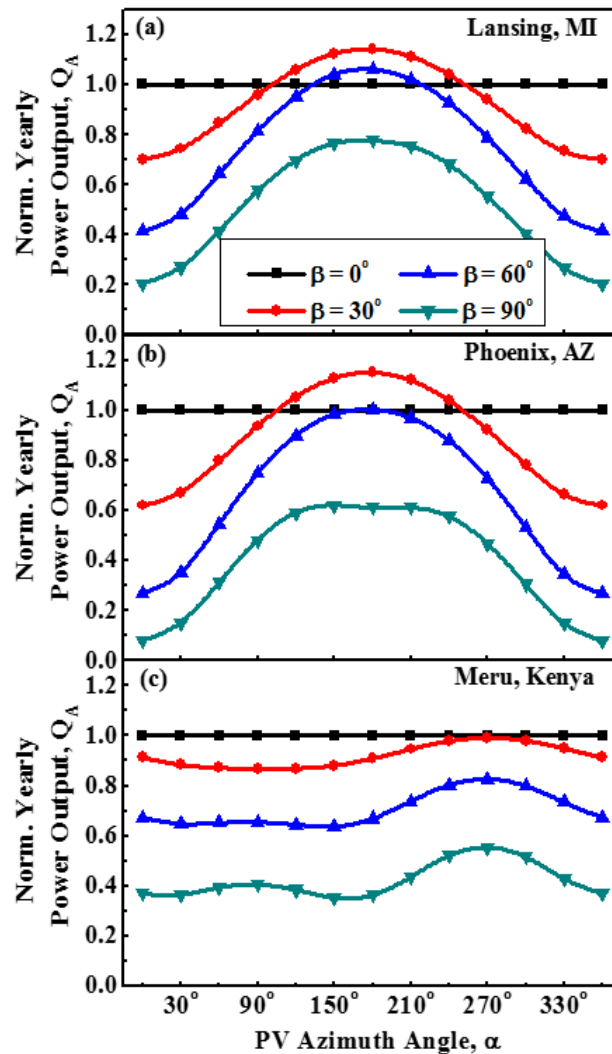


Figure 6 Normalized yearly power output of Device A at various orientations in (a) Lansing, MI, (b) Phoenix, AZ, and (c) Meru, Kenya. Note that the overall output yearly powers are normalized to the non-tilted (horizontal) configuration

direction; and the values are the same at the north-facing and south-facing directions. The divergence in the east-west symmetry for Meru stems from two phenomena: 1) the time that the sun is positioned in the southern and northern sky is nearly the same at equator, so the power output of the modules facing either south or north are similar; and 2) the irradiance is slightly stronger and the illumination period is longer in the afternoon than in the morning, which results in a greater power output for the west-facing direction than the east-facing direction.

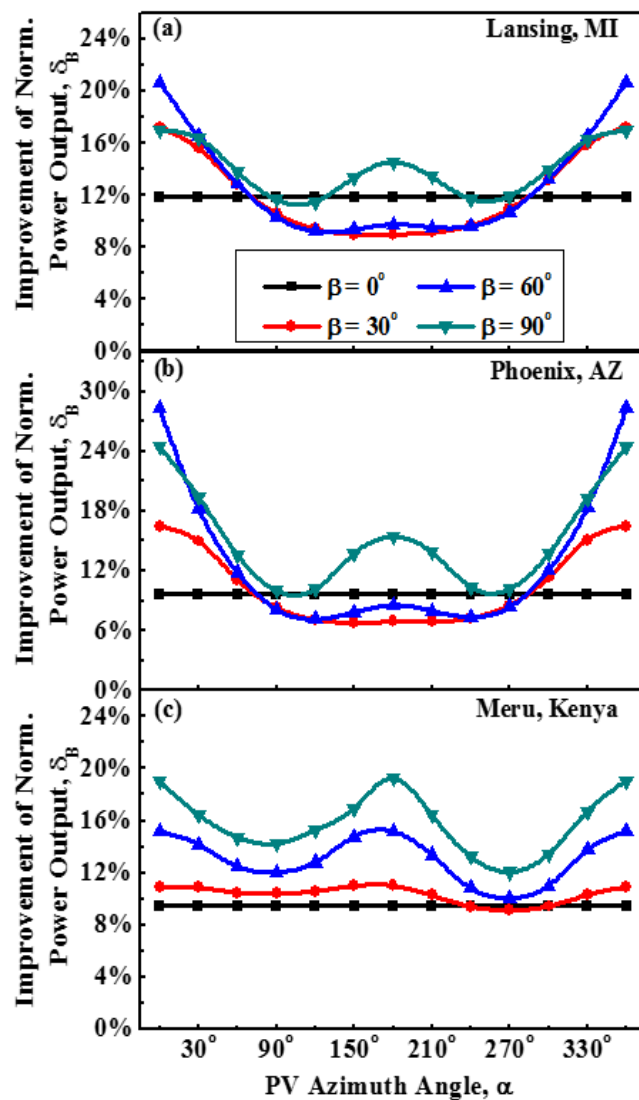


Figure 7 Normalized yearly power output improvement made by Device B in (a)

Lansing, MI, (b) Phoenix, AZ, and (c) Meru, Kenya

Figure 7 shows the improvement in power output by using device B (δ_B), which has minimal angle dependence, at various PV orientations for the three locations. An optimum enhancement appears at the north-facing and south-facing directions, which becomes more pronounced as the tilt angle increases from 30° to 90° for Lansing and Phoenix, and from 0° to 90° for Meru. Figure 7 clearly illustrates that the improvement in device B's angular dependence (highlighted with the blue area from Figure 4) significantly increases power output. For Lansing and Phoenix, θ is always very large for titled modules at the north-facing directions, so the improvement in power output exceeds that in the south-facing directions. However, the most beneficial orientations are still south-facing where the most direct incidence occurs. For modules with small tilt angle β at midday, the incident angle is also small such that the advantage of device B is less significant (Figure 4). In contrast, for a large module tilt (e.g. vertical orientation), the incident angle θ would be greater than 40° at midday [28], where the difference of responsivity between device B and A begins to emerge and the illumination is the strongest, so the overall power output is greatly enhanced with improved angle dependence. Since the solar irradiation is larger at a lower latitudes, the improvement (δ_B) is more substantial in locations such as Phoenix and Meru. This data ultimately highlights that the angle dependent performance plays a large role for a range of orientations in BIPVs that can translate into substantially enhanced power outputs or equivalently to higher efficiencies.

To further generalize the impact of cutoff angle in the angle-dependent PV design, additional simulations for hypothetical modules with sharp responsivity cutoff angles (40° , 55° , 70° , 80° , and 90°) with several selected tilt angles were performed using the solar irradiance data from Phoenix. Figure 8 shows that: (1) for horizontal and low tilt angle ($< 30^\circ$), the critical cutoff angle (where total output drops by more than 20%) is in the range of θ around $55^\circ - 70^\circ$ so that

good responsivity at very oblique incident angles is less significant; and (2) for highly tilted modules, the key cutoff angle becomes greater (θ around $70^\circ - 80^\circ$) so that this effect is more substantial, and good responsivity across all incident angles is highly desirable. It is also clear that larger cutoff angle result in more uniform power output for deployment over a full range of azimuthal rotations than smaller cutoff angle at tilted configurations. For cutoff angles below 55° , the reduction is particularly severe for south-facing directions ($\alpha = 180^\circ$), actually resulting in less power output than from east-facing and west-facing directions. Hence, reducing or eliminating the angle-dependent roll off of θ up to at least 70° is a reasonable target for maximizing power output in a range of deployment conditions.

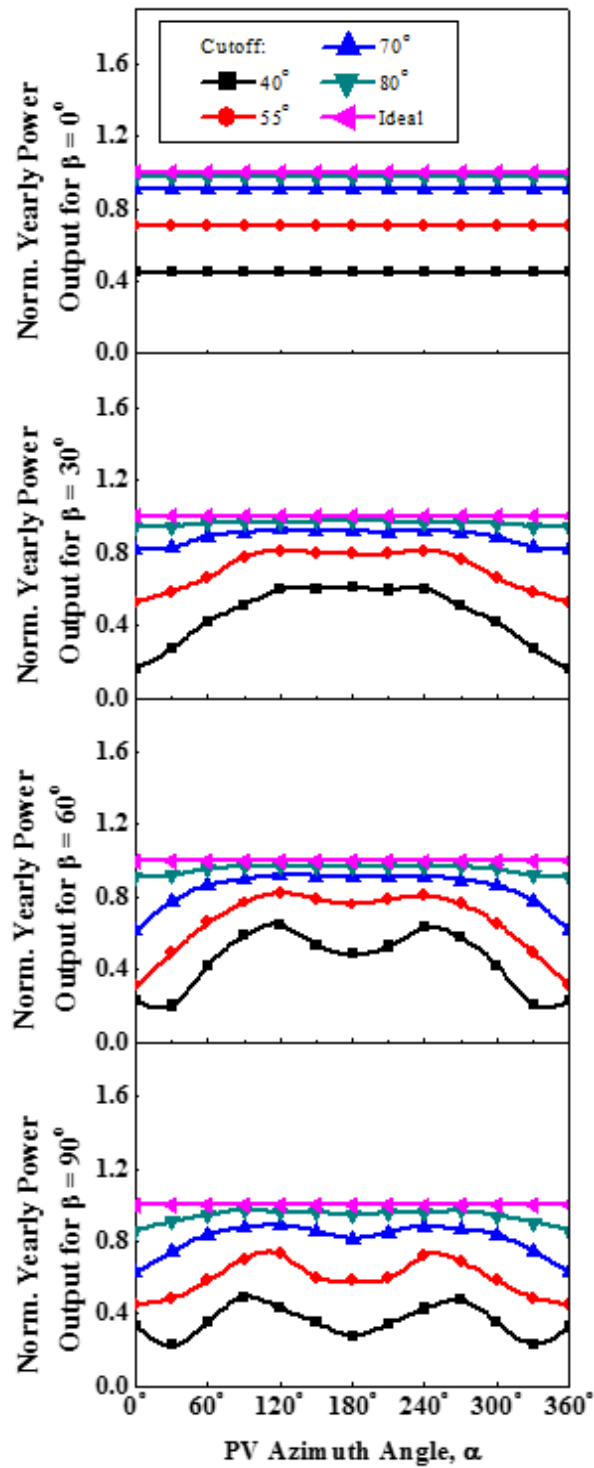


Figure 8 Normalized yearly power output for idealized responsivities with sharp incident-angle dependent cutoff performance with modules at various tilt angles in Phoenix, AZ

CHAPTER 2

Energy Saving Building Renovation Studies

2.1 Introduction

SPARTA is structured to have three teams to work on three building retrofit areas from both energy generation and energy conservation stand points: building-integrated photovoltaics, window film application, and LED lighting renovation. Solar energy is a target renewable energy source currently being considered by MSU. As it is well known, solar energy can be used for both for heating and direct electrical power generation. Findings from the 2010 Black and Veatch report [29] concluded that technologies like solar air conditioning and solar water heating are unfavorable, both due to the high capital expense of back-up systems and the subsequently low cost of the campus' central-controlled steam and water system. Solar energy for the use of power generation on the other hand does not bode so poorly. Using solar energy to generate electrical power will be a good option in the near future especially as it becomes more financially feasible to purchase and install systems. As a means of showcasing the interest in solar energy, MSU has contracted out the installation of a 250 kWp solar panel system on the roof of the MSU Surplus Store and Recycling Center, and at peak generation, it is able to supply 10% of the building electricity load [30]. Although Lansing does not have the most ideal solar radiation conditions, nor nearly as sunny days like that of southern locations like Phoenix, Arizona where the yearly average solar radiation of 3.8 kwh/m²/day comparing to 5.8 kwh/m²/day on a horizontal surface, it is still very likely to make a significant contribution to the 100% renewable energy goal, especially with the current solar technologies and massive space on campus including building façade, rooftop, carport, and ground mounted configurations. However, it is difficult to estimate the total power generation potential due to some physical constrains such as land use planning and roof type, which is unique to each open land area or building. Therefore, it is necessary to study the total viable space still in details.

While using alternative energy sources for power generation, reducing energy consumption is another focus to pursue sustainability. It is obvious that most of the power generated is supplied to hundreds of buildings on campus, so improving building energy efficiency will greatly reduce energy consumption. MSU has participated in the Better buildings Challenge, a national leadership initiative through the US Department of Energy, and committed to improve building energy efficiency at least 20% by 2020 [31]. The greatest potential energy saving area for a building is lighting[32]. With light emitting diode (LED) technology, the power consumption per light bulb can be reduced more than half. Considering the massive amount of light bulbs in a building and the operating hours of these light bulbs in the public area such as hallways and classrooms, the accumulated saving over time can be extraordinary [33]. In addition, the retrofit could be completed without changing the original electrical set up, and the outcome is easily monitored to prove the impact from replacing the fluorescent lights to LED lights. Along with the LED retrofit window film is a relatively simple application to reduce building energy load. It works by preventing the solar heat from penetrating through glass doors and windows into the buildings. Users just need to apply the film onto either interior or exterior of existing windows, which is more cost effective than replacing with low-e windows. Although other window technologies such as blinds and mesh screens can largely reduce solar heat transfer as well, they will block the view and increase the indoor lighting usage. Nowadays, window film can be made to have high visual light transparency and heat insulation. It not only can save energy by as much as 33% [34], but also increase aesthetic appearance of buildings and occupants' psychological health[35]. Depending on the building structure and window area, the energy saved by cutting off solar heat can be very different. Therefore, it is important to evaluate the window film application for the buildings on campus.

This chapter focuses on the solar energy generation from rooftop solar panel installation and solar heat reduction from window film application. It assesses the impact of these building integrated solar technologies from computational modeling on several case studies.

2.2 Rooftop Solar Panel Installation

2.2.1 Module Design and Operation Background

A typical module consists of a number of solar cells connected either in series or in parallel to build up the desired current or voltage. Typical solar cells are usually 156mm x 156mm in area, and encapsulated in ethyl vinyl acetate or glass (used as a top surface) and Tedlar (used as a back surface). The top surface of a cell must have a high transparency and a low level of reflection for light to be absorbed. Cells must also be high-impact and water resistant in order to protect the metal contacts and interconnects from being damaged under various weather conditions. In addition to these features, the back surface needs to have a low thermal resistance because an accumulation of heat exposure will also act to reduce the lifetime of the module.

Electrical mismatch occurs when the interconnection of solar cells do not have identical short-circuit current or open-circuit voltage, which causes power loss at the module level. When solar cells are connected in series, the voltage mismatch does not affect the overall current but the overall voltage will decrease, which resultantly reduces the overall power generation capability of the panel; the current mismatch will reduce the open-circuit voltage logarithmically, which may cause large power losses due to the fact that the overall current is equal to the lowest level current in the series. When solar cells are connected in parallel, the current mismatch is actually quite trivial. Instead, the voltage mismatch will reduce the overall open-circuit voltage; but this issue is not very significant at the cell level.

Shading part of a cell will cause a module's current and power output to decrease. This resulting power loss is directly proportional to the amount shaded area a cell is exposed to. Each module can be connected in parallel to build a *block* or in series to build a *string*. When a module of a string-connected block happens to be partially shaded, which is equivalent to a current mismatch of series-connected solar cells, the overall current output and power output of that block will decline proportionally each block's shade exposure. When only a small portion of the modules in series are shaded and a large amount of modules are unshaded, and the unshaded modules are likely to create what is called reverse bias on the shaded modules such that overheating occurs at the shaded modules leading to irreversible destructive effects.

Solar cells will absorb part of the light that is below the band gap and convert that to heat. The heat usually cannot be transferred out of the module efficiently enough so that the temperature of the module will increase. This will reduce the voltage output, accelerate degradation, and induce thermal expansion. For example, for each 10 °C increase in temperature, the degradation rate will increase by a factor of two [36].

Manufacturers may warrant up to 25 years of PV modules, but degradation and failure could still occur. The short-circuit and open-circuit failures at cell level of module level are often results of manufacturing defect, corrosion by water vapor, and weather conditions. Cracking is also a common failure mode due to non-uniform thermal stress distribution. The reversible reduction in output power happens when the module is shaded by surrounding objects and the cumulated dust on top surface. Other failure modes include by-pass diode failure, encapsulate failure, module delamination. All the reasons mentioned above could decrease the lifetime and lower the performance of PV modules.

2.2.2 MSU Rooftop Solar Energy Capability Assessment

Michigan State University has a fairly large land area of approximately 21 km² consisting of 2100 acres in existing or planned development, including 538 buildings where 95 of which are academic buildings[37]. Due to issues with confidentiality, only 192 buildings' blueprints were archived and surveyed. The survey documented the roof structure type such as flat and sloped, the area of each roof section of a building, and determined the facing direction when the roof sections were sloped. When the roof section is either north-facing, 50% shaded, or smaller than 300 ft², the section is excluded in the total viable area calculation for economic feasibility concerns. The survey results show that 174 buildings have suitable roofs for solar installations, including 82 flat roofs, 80 sloped roofs, and 12 combined roofs. Amongst the flat and sloped roofs, 28 buildings have been found to not be suitable due to either small amount of accessible area or heavy shading coverage. All of the surveyed buildings together provide 335500 m² flat roof area, including 25900 m² south-facing roof area and 40300 m² east or west-facing area. The potential power generation alone, from this accessible flat roof area would be upwards of 11 MW when using 20% solar cell efficiency, which is roughly equivalent to 17.5% of the university's historical peak demand of 63 MW [38]. Note that this is derived through the estimation of annual average solar radiation in Lansing, which is 3.83 kWh/m²/day [39].

Seeing as campus buildings have been built over a significant time period, from the early 1900s to now, the roof structures that exist on campus have wide range of diversity. The most commonly seen roof types are slate, metal, and inverted membrane, in either sloped or flat configurations. The slate roofs typically seen in the earlier constructed buildings are composed of very expensive materials and expected to last beyond 100 years. Mostly due to the extensive replacement costs, roofs of this kind have been rated as unsuitable for solar panel installations.

Metal roofs, on the other hand, are under consideration. The 40 kWp MSU Surplus Store and Recycling Center rooftop array sits atop a steel tube metal deck roof, and because it is strong enough to support weigh load, it remains a good candidate for further consideration. However, the disadvantage of considering metal roofs for panel installations is that the metallic thermal expansion at the change of temperature may cause roof leaking issues at the sites where arrays are fastened to the roof deck. Due to this among other, foreseeable, constraints, metal roofs are not ideal, but nonetheless remain as a viable space for rooftop solar arrays. The inverted membrane roof type for rooftop mounting systems remains possibly the best candidate, both due to its rigid concrete structure, allowing it to easily accommodate the weight of the array and the stone ballasts, and the membrane's water proofing qualities, allowing it to seal and insulate against leakage issues, unlike that seen with the metal roofs.

In order to take a closer look at each surveyed building, they are ranked based on a building based scoring criterion known as the Array Impact Metric (AIM), which is the maximum viable roof area in square feet for solar panel placement per MWh of fiscal year 2014 electricity consumption of each building. The greater AIM score makes the building be a more attractive candidate for conducting studies on. The ranking will help identify those buildings that are more economically feasible targets for future analysis with the solar planning tool. The full list of the buildings which have a viable roof area greater than 6000 ft² is available in Appendix I.

2.2.3 Solar Deployment Analysis Software

Currently, existing photovoltaics installation modeling tools have their own strength in pre-feasibility, sizing, and simulation [40]. The pre-feasibility tools are usually for first time assessments that have more details in financial impact such as tax credits and government incentives. The sizing tools would output the most effective size of each given component such

that the levelized cost of energy is minimal, but the financial analysis may be missing. The simulation tools can calculate the energy generation and system losses as a function of time, and it usually involves in complicated inputs that requires intensive understanding of both PV system and balance-of-system. Most importantly, usage fees for the software are too expensive.

SPARTA has developed a solar planning tool for MSU that can automatically size a PV system for a given area with MATLAB program[41]. The tool outputs the total number of panels and overall yearly power generation using TMY 3 hourly data. The benefits of the tool are that it avoids the shaded area created by surrounding objects when sizing up a system and it can combine different sections together as a whole system. The restriction is that the input requires a 2-dimension well-defined area blueprint in an image format. However, the work required to get a good blueprint before running the simulation is massive, and the interface is not very user-friendly, which raise the need to seek for an alternative.

HelioScope[®], developed by Folsom Labs, is the alternative software that SPARTA utilized in parallel. It was both used to validate the software developed previously and used to help visualize solar planning tools moving forward. It is an advanced PV system planning tool for commercial and residential designs that integrates Google maps and Sketch Up for detailed system designs along with other performance modeling into power a generation analysis to improve the process of solar array designs. It is a component-based model, which aggregates separately modeled sub-systems together into a full system, providing configurations that closely resemble the real-world behavior of solar arrays. Aside from its very user friendly interface, the results provided by HelioScope[®] fall within 1% of PVSyst modeling results (a widely used design tool in the solar industry).

Users can locate an area using Google Map, and then draw the system boundary of the solar array over the map background. This includes the capability to identify keep-out areas within the boundary. By either entering the height of keep-out areas or inputting a Sketch Up 3D drawing of the surrounding environment, HelioScope[®] is able to generate shade projections for the layout design. In addition, HelioScope[®] has a large selection of solar modules, including the module performance and other important specifications. After the layout design, the system model can simulate the full system's electrical relationships including inverters, combiner boxes, wires, and distributed electronics, which are user-defined inputs, and the selections over the different electrical components and configurations will render results to show percentage losses over each component. When modeling the power generation, three common models are available: a single-diode model, a PVSyst model, and a temperature model. HelioScope[®] also uses regional meteorological data files such as TMY3 for the irradiance calculation. It allows for the incorporation of optional environmental effects such as irradiance adjustments, near shading, and other mismatches into the simulation runs.

2.2.4 Case Study of Wells Hall

Wells Hall, a good candidate building, has been selected for a detailed HelioScope[®] analysis. The roof sections are flat, and have different elevations across each section (Figure 9a). The total area is 55126 ft² (5121 m²) read from the blueprint. The Solar module used for the simulation is the Suntech STP210-18/Ub 210W mono-Si. The panels are tilted at a fixed 33° and are facing south, or an azimuth of 180°. To avoid intrarow shading from panel strings, spacing is calculated to be 5.51 ft using occurring on December 21 from 10 am to 2 pm. During this time, some lower roof section areas are shaded, so the placement of solar panels is avoided in that region (Figure 9b). The selected inverter is the Siemens SINVERT 100 M-3DC 105kW. To reach a useful

voltage and current, 22 modules are combined into a string to generate a V_{OC} of 739 V, and 12 strings are combined to a combiner pole to generate a current of 409436 A. The wire for each

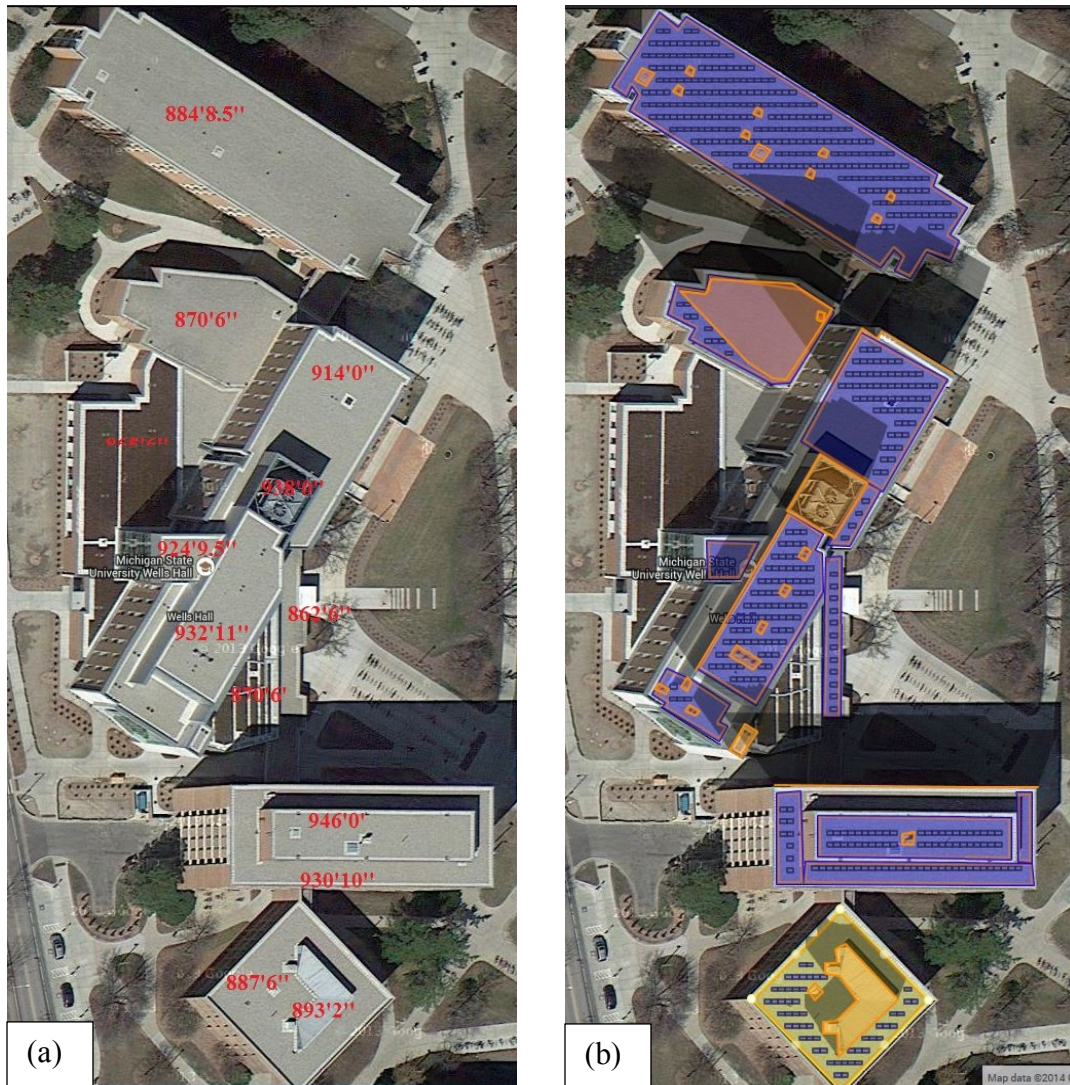


Figure 9 (a) Wells Hall elevation map, (b) Wells Hall solar panel layout

string and connection to combiner is 10 AWG copper wires. Therefore, a total number of 421 solar panels can be installed to generate 147.7 MWh (120 kW DC) electricity annually. At peak load, the electricity output is 1229.5 kWh/kWp. A full report by HelioScope[®] is available in Appendix II.

To prove out financial feasibility, the national capital-weighted average non-residential system price was used at \$3.72/W [42]. Using this value, the total installation cost of the Wells Hall project is \$348,618 including direct/indirect capital costs and a 6% sales tax. Regardless of the salvage value at the end of its warranty, the annual system depreciation is \$14,945. Using the current average electricity rate of \$0.093/kWh at MSU with 1.74% inflation rate and annual electricity production of 147.7 MWh with 0.5% annual system degradation rate, the total financial savings is \$404,732 over the 25 warranted years of operation - and this would also see an annual cash flow rate of \$15,516 assuming 3.5% real discount rate. The payback time therein would be 22.5 years with a Return-on-Investment (ROI) of 11%. The simple financial calculation above showed that solar energy at Wells Hall does not seem to be currently attractive enough to outweigh the high capital expense the project would require. However, as the electricity rate continues to increase and the solar module price and Balance of System (BOS) costs continue to decrease, solar as a clean and renewable energy could be a great option to power the campus in the coming future.

2.3 Low-e Window Film Energy Saving Study at Kresge Art Center

2.3.1 Properties of Window and Window Film

Window film is a viable technology to prevent solar heat from being transmitted into the room and to reduce the Sun's glare. When the solar radiation is filtered by the atmosphere, it typically consists of a 3% ultraviolet region, a 38% visible region, and a 59% near-infrared region. The ideal material for use in windows would allow most of the visible light to pass through, while absorbing all of the infrared light, but the standard 1/8 inch thick single-pane clear window glass is far from ideal. The windows installed on many campus buildings only reflect 8% of incoming solar radiation to the outdoors, while absorb only 6%, and transmit 86%

indoors. These numbers do not change much within the 0° to 60° incident angle range. The light that comes through the window may be absorbed and reflected by the many other indoor surfaces, eventually getting absorbed by the rooms' objects. Consequently, often by way of low performance windows, solar radiation introduces heat into a building and raises the indoor temperature.

The solar heat gain coefficient (SHGC) is a term that describes the percentage of the incident solar radiation being transmitted into the building through windows. The installation of window film usually does not affect the thermal resistance of the window, but it reflects a large portion of solar radiation outdoors. Some window films reflect all regions of the incoming solar radiation, but they typically appear as a dark tinted color, which is displeasing to the occupants and requiring an increased reliance on artificial lighting. Some window films are able to selectively allow visible light to go through and absorb near-infrared outdoors, which remains the transparency of the original window, while still reduce the total solar heat transmission by as much as 60%. Besides, 99% of UV lights, which is harmful to furniture and human, can be filtered. In cold climates, the windows should have the highest transmissivity and indoor far-infrared reflectance as possible, but due to the less effective heating system than cooling system, window films that reduce solar heat are still helpful. In warm climates, however, the windows should block the infrared region while letting visible light to pass through, so as to maintain good lighting conditions. Comparing to the clear glass, additional window film layers may lower the cooling load by 15% to 30%. Depending on the location and purpose, it is important to choose the correct window film for the setting.

2.3.2 Cooling System Modeling and Calculation

RESFEN, developed by the Lawrence Berkeley National Laboratory, is widely used in the industry to calculate the heating and cooling energy effects of windows in residential buildings. It has libraries for windows, building envelopes, climates of specific locations, and utility rates. Users are able to adjust the floor area, window area, window orientation, interior/exterior shading, window properties, etc. However, due to some restrictions and assumptions embedded in RESFEN such that users have less control on these inputs, it is not suitable for MSU's campus buildings such.

Hourly Analysis Program (HAP) is a HVAC system designing tool for commercial buildings and also provides energy analysis of buildings regardless the size and functionality of the building. It follows the calculation procedures by American Society of Heating, Refrigerating and Air Conditioning Engineers (ASHRAE) and it is accepted by the U.S. Green Building Council the use of performance calculations in the LEED Rating System.

It adds more freedom to the users to define input parameters, with the most commonly adjusted inputs of size and thermal properties of the space, the type of air handling systems in use, the cooling and heating system, and the use of the space including scheduling and type. It also provides access to multiple hourly weather databases for the use in energy simulations, such as the TMY worldwide, which enables a more detailed study as compared to RESFEN.

The heat transfer principles used in the software are universal. The heat transferred (\dot{Q}_{trans}) into a room consists of ventilation (\dot{Q}_{vent}), natural convection from the floors, ceiling, walls, windows and doors (\dot{Q}_{conv}), solar heat (\dot{Q}_{solar}), and heat generated by the occupants (\dot{Q}_{occu}). Here is a modified version following the ASHRAE calculation procedure (Cooling and Heating

Load Cal Manual), it has been provided to account for the cooling load requirement of an office based space:

$$\dot{Q}_{trans} = \dot{Q}_{vent} + \dot{Q}_{conv} + \dot{Q}_{solar} + \dot{Q}_{occu} \quad (\text{Eq. 7})$$

The heat transferred by system ventilation is caused by the temperature difference of the air coming from the outdoors, and it is calculated by

$$\dot{Q}_{vent} = \dot{m} \cdot C_p \cdot (T_2 - T_1) \quad (\text{Eq. 8})$$

where \dot{m} is the air mass flowrate ($\dot{m} = \rho \cdot \dot{v}$); C_p is the heat capacity of the moisture air; T_2 is the outdoor temperature and T_1 is the indoor temperature. \dot{m} and C_p can be assumed to be constant since the change due to temperature, pressure and moisture is not very significant when considering air gas. When $T_2 > T_1$, heat is being transferred into the room, so \dot{Q}_{vent} will end up having a positive value.

The natural convection of this process is mostly occurring at the wall and windows in contact with the outdoor environment and the temperature gradient is typically large. This is calculated by

$$\dot{Q}_{conv} = (T_2 - T_1) \sum (U_i \cdot A_i) \quad (\text{Eq. 9})$$

where U_i is the overall heat transfer coefficient or the U-factor of either floor, ceiling, wall, or door, and A_i is the corresponding area.

The solar heat transmitted into the room depends on the SHGC, the irradiance, and the incident angle as

$$\dot{Q}_{solar} = SHGC \cdot I_{GT} \cdot A_{window} \quad (\text{Eq. 10})$$

The cooling load reduced by applying the window film (\dot{Q}_{save}) can be calculated from the difference in solar heat transmission:

$$\dot{Q}_{save} = (SHGC_{w/ofilm} - SHGC_{wfilm}) \cdot I_{GT} \cdot A_{window} \quad (\text{Eq. 11})$$

The occupants' heat includes the people and electronic equipment such as printers, computers and lighting. These values vary significantly and need to be carefully estimated for each specific situation. Provided with these values, a simple equation to calculate the electricity consumption (P) of a window AC unit then is

$$P = \dot{Q}_{trans}/EER \quad (\text{Eq. 12})$$

where P is in Watts; \dot{Q}_{trans} is the cooling load in Btu/h; EER is the energy efficiency ratio rated by the manufacture of the window AC unit (Units for this measurement are in Btu/Wh).

2.3.3 Window Film Case Study at Kresge Art Center Results and Discussion

MSU Kresge Art Center building room 113 was selected for the window film case study. This space was selected because it is a confined space with window air-conditioner whose energy consumption can be easily measurable. The area is an open office space, connected centrally to other air-conditioned rooms on the same floor. The space has a floor area of 278 ft² and one occupant who uses the space during regular office hours, i.e. 8hr work period. It is assumed that the air is stagnant, and the temperature of the surrounding indoor rooms is as the same as that space. Therefore, it is assumed that heat transfer does not occur between any of the indoor rooms on the same floor, but only between the outdoor and indoor environment and the unconditioned floors above and below. The room has a south-facing wall of 42 ft² including 68 ft² of window area. The overall U-factor is 0.295 Btu/(ft²-h-°F) for the wall, and 0.1 Btu/(ft²-h-°F) for the floor and ceiling. The windows are clear single-pane glass with an aluminum frame, and

the U-factor is 1.2 Btu/(ft²-h-°F) with SHGC of 0.8. After the window film was applied, the SHGC dropped to 0.5. The temperatures used in the simulation are between 66 – 78 °F for the unconditioned indoor space, and 65 – 95 °F for the outdoor environment. Also, the average dry bulb and wet bulb outdoor temperatures hover around 86.6 °F and 72.3 °F respectively, and the conditioned room is assumed to be maintained at 75 °F. The ventilation system including supply and return line were selected in the modeling. To emulate realistic conditions, central heating was also selected, but the cooling system was altered to reflect the use terminal units with a packaged DX fan coil. In this case, the default ventilation rate was 22 ft³/min of outdoor air supplying the room.

Table 1 HAP modeling results

Zone Loads	Details	Before Window Film		After Window Film	
		Sensible Heat (Btu/h)	Latent Heat (Btu/hr)	Sensible Heat (Btu/h)	Latent Heat (Btu/hr)
Window Solar Loads	56 ft ²	3170	--	1981	--
Wall Transmission	42 ft ²	72	--	72	--
Window Transmission	56 ft ²	543	--	543	--
Floor Transmission	278 ft ²	-50	--	-50	--
Ceiling Transmission	278 ft ²	-50	--	-50	--
Overhead Lighting	136 W/fixture	348	--	348	--
Electric Equipment	200 W/equipment	606	--	606	--
People	1	168	205	168	205
Return Fan Load	461 ft ³ /min	0	--	0	--
Ventilation Load	22 ft ³ /min	250	58	250	58
Supply Fan Load	461 ft ³ /min	0	--	0	--
Total		5057	263	3868	263

The results show that the most impactful region of heat transfer came predominately from the solar heat through the windows (Table 1). Before the window film was installed, the solar heat

transfer rate, the heat due to occupants, and the heat due to ventilation was 3170 Btu/h, 1327 Btu/h, and 250 Btu/h, respectively. The heat transmitted from outdoor environment through both the window and walls were 534 Btu/h and 72 Btu/h, respectively. However, heat was being lost from the floor and ceilings at a rate of 50 Btu/h. Thus, the total heat transfer rate was 5320 Btu/h. After the window film was installed, only the solar heat transmission decreased to 1981 Btu/h while the rest of the heat transfer values remained the same. Thus, the total heat transfer rate dropped to 4131 Btu/h; equaling a reduction of 22%. However, the ventilation rate that was measured to be on average 512 ft³/min other than the default 22 ft³/min, and the air had 60% -80% moisture, which had a heat capacity of about 0.244 Btu/lb-°F. With these conditions, the heat transfer rate due to ventilation would be 1529 Btu/h using a 3 °F difference between the ventilation air temperature and indoor temperature. This dramatically weakened the impact of the solar heat gain reduction brought on by the film. Therefore, the window film application becomes less attractive for the type of room that has an abundant amount of air circulation (

Figure 10).

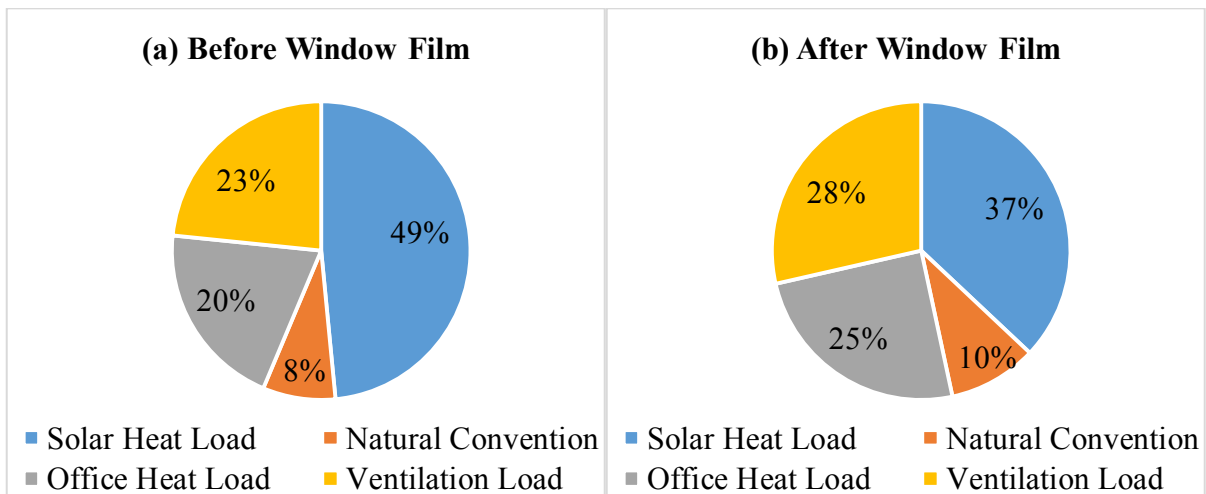


Figure 10 Heat transfer distributions (a) Before window film application; (b) After window film application

From the above simulation, the cooling load saving was 1189 Btu/h thanks to a 40% solar heat gain reduction. For a window AC unit that has an *EER* of 10, the power consumption will decrease by 119 W, which was equivalent to about 2 W per ft² per 10% SHGC reduction. Assuming 480 operating hours (40 hours per week times 12 weeks) of the AC unit for a summer, the total energy saving was roughly 57 kWh, resulting in \$5.30 of saving in electricity consumption cost using the \$0.093/kWh flat rate provided by the MSU IPF. The cost of window film projects including installation can range from \$5 – \$15 per square foot. For the high transparency film such as 3M PR70, the cost is close to the higher end of this range. Using Kresge Art Center room 113 as an example, the total installation cost was \$880 for the 56 ft² window area, which generated a payback time period beyond 100 years. From this we can expect that, financially speaking, window films in high latitude regions are typically not going to be ideal when the focus is a payback from reduction in cooling load, even on the south-facing windows where expose to the most solar radiation.

On the other hand, feedback from the occupants verified that window film can largely reduce the glaring on the computer screens as well as enable a view of the outdoors, which enhances the comfort and work productivity. For these reasons, window film dose offer some advantages to improve peoples' psychological health and work productivity.

2.4 LED Lighting Retrofit at Psychology Building

2.4.1 Light Fixture Selection

The light fixtures across campus are mostly fluorescent lighting. However, newer lighting systems such as light emitting diodes and organic light emitting diodes offer substantially higher efficiency, but with higher bulb and installation cost. In this section we explore the potential of

these new lighting systems to replace existing fluorescent systems, analyze the energy impact and cost payback.

Table 2 A Comparison of CCT and CRI of F32T8 and CREE UR 2 LED light fixtures[41]

	CCT		CRI		
	Manufacturing Data	Measured Data from Spectra	Manufacturing Data	Measured Data from Spectra	Calculated at Declared CCT
F32T8	4100 K	3700 K	78	82	65
CREE UR2	4000 K	3800 K	80	84	87

The fluorescent bulbs widely used on campus are the F32T8 model. In order to find a good replacement of the current fluorescent light, the correlated color temperature (CCT) and color rendering index (CRI) of selected LED light need to be matched. SPARTA has measured both values of F32T8 and a full range of LED light fixture options, and CREE UR2 stood out for its better light quality and being exceeding the performance of the existing light condition (Table 2). The results show that the CRI of F32T8 has decreased from 78 to 65 at declared CCT of 4100 K, while the minimum requirement for interior lighting should be 80 [43]. On the other hand, CREE UR2 has a CRI of 87 at declared CCT, which makes it more favorable than fluorescent light. Another reason to choose CREE UR2 is that the CREE bulbs have a good design for longevity by separating the drivers, which avoids the premature failure of the bulbs due to the heat produced by the driver and provides the best warranty (7 years). In addition, the power consumption for the CREE fixture with 2-light bulb is only 44W while that of the F32T8 fixture with three bulbs is 110W, which is more than half saving on energy. Although the capital expense per LED fixture is about 15 times more expensive than fluorescent light fixture, it still can be a profitable investment when combining the benefits of good CRI and CCT, long lifetime,

and less power consumption that LED light provides, which are all critical to finding a viable adoption option that the University would support.

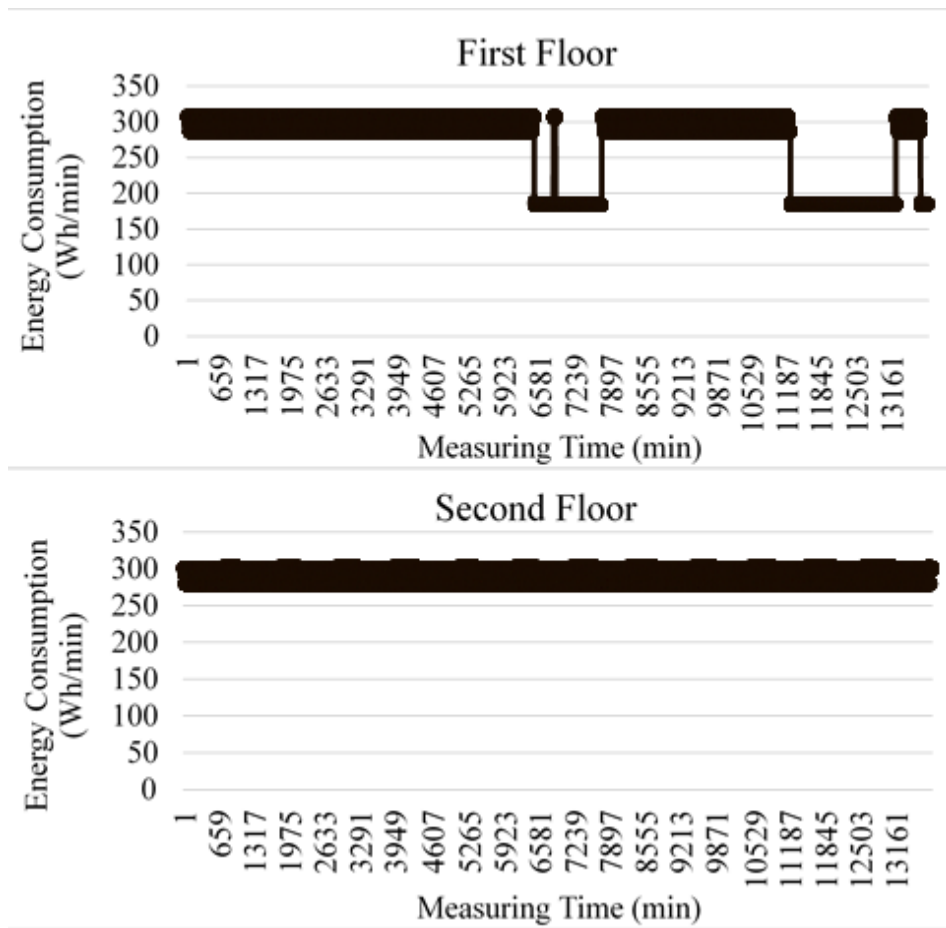


Figure 11 Monitored energy consumptions of current fluorescent lights at Psychology Building

2.4.2 Financial Analysis for Psychology Building LED Retrofit

SPARTA has conducted a small-scale project at the hall ways on the first and second floors of Psychology building to demonstrate the impact of the LED retrofit. This building is selected because of the great amount of the fluorescent lighting fixtures and the long operating hours according to the walk-through survey done by SPARTA members, which could potentially leads to a large impact on energy saving. By doing in depth monitoring, there are 91 F32T8 fixtures in

total and they are turned on 100% of the time (Figure 11), which consumes 86.7 MWh electricity annually. If all the 91 fixtures were to be replaced by LED, the electricity consumption by lighting will be reduced to 46.3 MWh, which is reduced by 46.6%. The total cost including installing would be \$11,327, but the payback time and total cost saving would be 2.94 years and \$44,875 over the lifetime of the LED fixtures of 10 years (Table 3).

The sensitivity analysis uses the condition in Table 3 as a baseline and alters installation time, light fixture price, operating time, and escalation ratio (Figure 12). The results show that the operating time of the fixtures is the most effective parameter on payback time. When the operating time is greater than 22 hours per day, the payback time would be shorter than 3 years; when the operating time is 12 hours per day, and the payback time would increase to 5 years. Nonetheless, LED retrofit is a cost-effective way to reduce energy consumption and expense.

Table 3 Financial analysis on Psychology Building LED retrofit

Installation Labor Time (min)	60
UR 2-48 Pricing (usd)	\$90.12
Annual Utility Rate Escalation (Average, %)	1.44%
Inflation Rate (Average, %)	1.74%
Real Discount Rate (%)	3.50%
Time Fixtures are on (Average, %)	100%
Degradation (%/year)	1.00%
Expected Returns (kW)	5.28
First Year Annual Savings (kWh)	46,262
First Costs	\$11,326.85
Adjusted Installed Costs	\$11,326.85
Payback Time (yrs)	2.94
Lifetime NPV (10yrs)	\$18,406

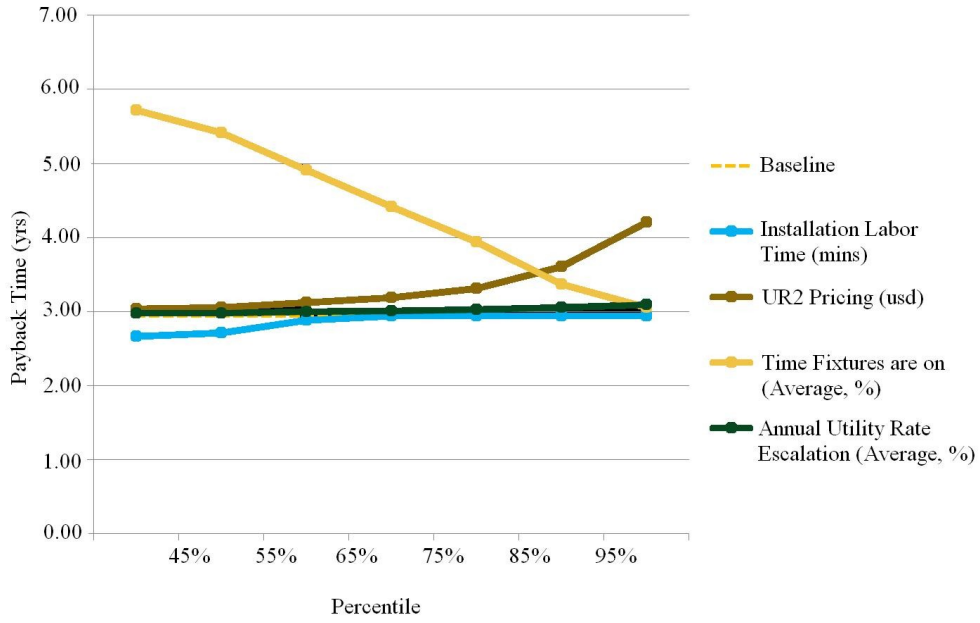


Figure 12 Sensitivity analysis of LED lighting

CHAPTER 3

Outreach Activity – Engaging Students

3.1 Introduction

The SPARTA group was tasked not only to analyze and implement renewable energy technologies, but also to educate the campus and public on renewable energy technologies. While solar energy has been under the spotlight for the past few decades in the research community, and silicon based solar cell technology has become more widespread, the high cost of solar energy still continues to slow the implementation of solar energy. The idea of luminescent solar concentrators (LSCs) has existed since 1970s in the solar energy field of research, and the aim is to reduce the capital cost of solar energy and improve the efficiency of traditional silicon solar cells[44-46]. LSCs could be a very low-cost alternative to traditional photovoltaic technology as it allows current hurdles facing the industry along the lines of resolving issues with financial feasibility, making it very important to share this technology. Here, the developed a simple luminescent solar concentrator painting kit allows students to make their own LSCs that can generate electricity that are also art. To make this possible, we developed luminescent paints composed of multi-colored and blended dyes with different light absorption properties. In constructing these colorful and artful LSC systems, students are able to see the differences in power outputs instantly after painting and understand principles of waveguiding, and energy generation in a fun and interactive way. This chapter describes the designed classroom activities, the methods and materials development, and discusses the educational outcome.

3.2 Materials and Methods

3.2.1 LSC Architecture

The architecture of an LSC consists of a transparent plastic sheet, organic luminescent dyes, and strips of solar cells that can be attached to the sides of the plastic sheet (Figure 13). The dye

molecules usually have high quantum efficiency, and are either dispersed into the plastic itself or painted onto the surface of the sheet. The dyes absorb incident light and re-emit it at other

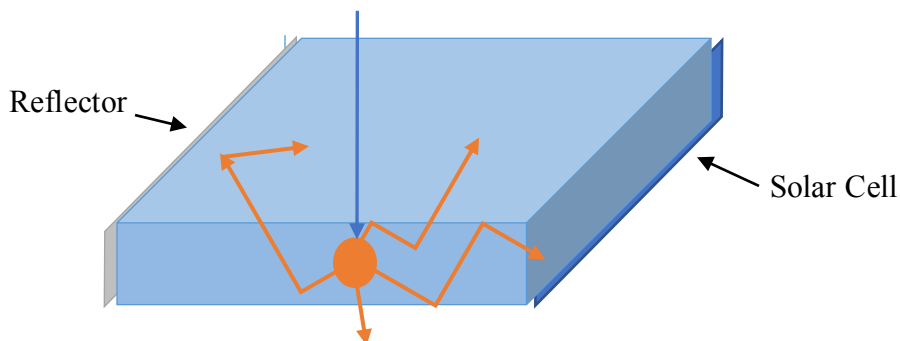


Figure 13 Luminescent solar concentrator architecture

wavelengths. The re-emitted light is then re-directed to the outer edges of the sheet through a process known as wave guiding, where the solar cells are attached, so as to harvest the redirected light. This process is made possible through the internal reflection of light that happens within the plastic sheet. By these means, the concentration of both direct and diffuse light can increase upwards 5 to 10 times of its original concentration values. The efficiency of the solar cell also increase due to the conversion of the solar spectrum into monochromatic light [44]. In comparison of a LSC to a typical solar cell with the same illuminated area, one would find that cost of the plastic sheet and the dyes together is notably cheaper than any traditional photovoltaic technology currently on the market, and not to mention the solar cell attached at the sides can generate more power than under the usual case of direct illumination. Due to the transparency of LSCs, they could potentially best be used for building integrated PV applications, like that of windows [15].

The concentration of the dye solution used significantly affects the power generation ability of the LSC. For a diluted solution, the emission increases with concentration in the dye, but above a critical concentration level, the emission is no longer improved by increase in

concentration. In fact, in some cases, losses in emission may be observed. This results from a high re-absorption by the dyes and low efficiency of amounts of emitted photons to absorbed photon [47]. Therefore, doing multi-layers of painting may not be necessary and may even cause losses in efficiency.

3.2.2 Procedure for Making Paints

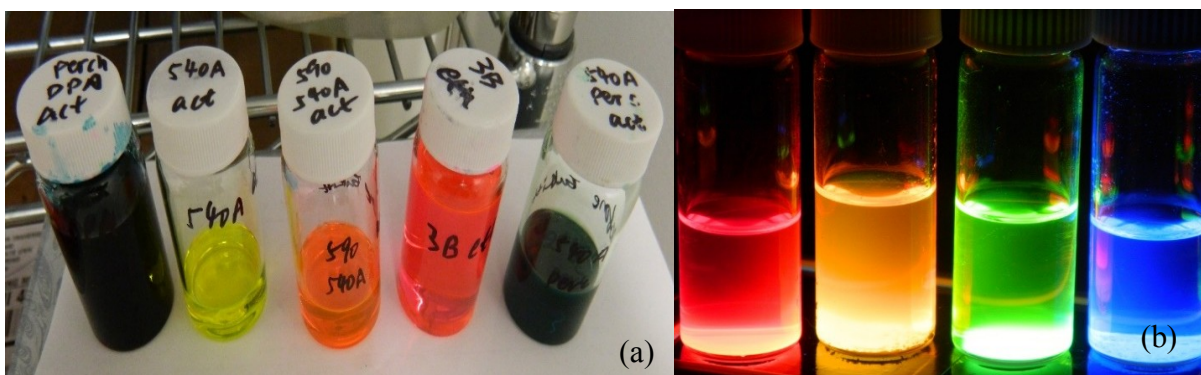


Figure 14 Finished paint solution samples (a) under room light; (b) under UV light

Generally, the compositions of the paints are just a dye compound, a solvent, and an adhesive material. The dyes need to represent a wide range of colors, and yield significant power output under either a flashlight or regular incandescent light bulb. Then, a proper solvent which has low toxicity and high solubility for each dye is also necessary (Table 4 and Table 5). This selection depends primarily on the desired color; the dyes can either be mixed together or diluted to form different colors. The color of the dried paint and paint solution can be dramatically different due to these factors, so it important to understand and pay close attention to the compositional components during solution making process. Under high energy light, such as ultra-violet, the paints will glow as shown in Figure 14. Eukitt (45% acrylic resin and 55% xylenes) is used as the adhesive material because it mixes well with most solvents and dries rather quickly, making it suitable for classroom activities. The ratio of Eukitt to the finished

solution is always 2:1. With an adhesive material, the dye particles are able to remain adhered to the plastic sheet after the solvent vaporizes.

Table 4 Paints recipe for using a single dye

Dyes	Solvent	Volume ratio of saturated solution to pure solvent	Color under room light	Color under UV light
540A	acetone	1:0	Yellow	Yellow
Rhodamine 590	acetone	1:0	Pink	Pink
Rhodamine 3B	ethanol	1:0	Rose	Rose
HITC Perchlorate SR-85	acetone	1:2.5		no
Rhodamine 590	ethanol	1:24	Pink	Pink
Rhodamine 640	acetone	1:50	Purple-pink	Purple-pink
DNP	acetone	1:0	clear	Lake blue

Table 5 Paint recipe for using mixed dyes

Solution 1	Solution 2	Volume ratio of solution 1 to 2	Color under room light	Color under UV light
540A	Rhod 590	1:10	Orange	Orange
540A	HITCP	1:1.5	Grass-green	Grass-green
HITCP	DNP	1:1	Light blue	Dark blue

3.2.3 Educational Kit Assembly

The educational kit consists of paints, plastic sheet, reflector, and solar cell frames (Figure 15). The plastic sheet is cut into a square and is combined with a plastic frame that is selected to hold the reflective mirror and solar cells in place. The advantage of having the frame is to make direct comparison of different colors of dyes without the misleading variations from a solar cell intermittent performance. The most challenge part is to cut the solar cell to the desired width such that it can fit into the plastic frame. The silicon solar cell comes in 156 mm x 156 mm dimension and is very fragile, and this is why the acrylic sheet with a thickness of 0.25 inch is selected. Also, to avoid the intricacy of soldering, conductive graphite glue is instead used to adhere the copper wires onto the top and back of the solar cell. The frame that holds the cell is also taped by off by black strips to prevent light from other space gap from being transmitted.

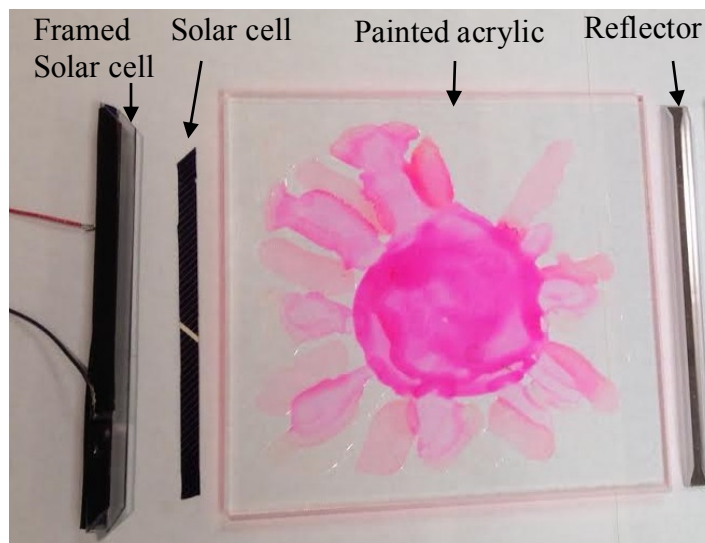


Figure 15 Education kit assembly

After the paint has dried, the sheet can be inserted into the solar cell frame and reflector device to test its power output.

3.3 Classroom Activity

3.3.1 Class Design

The participants are middle school, high school, and college students who are capable of following instructions to complete the paintings. The learning objectives are: (1) to illustrate the mechanism of LSCs; (2) to show the relationships between impact parameters such as light intensity and type of dyes as they are linked to power output; (3) to learn the power calculation using voltage and current.

The students are divided into groups, depending on the amount of materials that are available. Each student receives one clear plastic sheet and works as an individual. Two to three students can share the paints, but to avoid cross-containments, each paint brush must remain with its designated paints. Without telling the students which paint generates the most power, they are free to paint any patterns they want within a 5 minute period. While drying the finished paintings, the next group of students start, following the same exact procedure as the previous group. When testing the dried paintings, the same solar cell frame and light source must be used in order to eliminate biases. Multiple light sources can be used to illustrate differences in overall power generation, as determined by the intensity and wavelengths of the different form of light. The light source, such as a flashlight, is in contact with the sheet at the center of the painting, and the current and voltage outputs are recorded by a multimeter so as to calculate the power generated by the LSC configuration (Figure 17c). The solar cell can also be connected to a motor, and based on the speed of the motor, the power output differences can be easily demonstrated. The student whose painting has the highest power generation will be rewarded a gift such as a solar car model to take home.

3.3.2 Learning Outcome

A group of middle school students were participated in the classroom activity to learn about LSCs at Michigan State University's outreach day. After explaining the rules, most students started to paint as they would with regular paints (Figure 16). Within the 5 minutes time allotment,



Figure 16 Students at the painting station

the students were able to finish the painting quite adequately. Some students quickly realized that different dye colors output greater amounts power, and that the quantity of paint applied would have an effect on the power output as well. Some students used a single color while others used multiple.

During the testing, the students also learned the power calculation, which was helpful for them to remain rooted in the activity's scientific purpose. By moving a flashlight on the top of different colors, the students were able to make simple observations regarding the intensity of the light emitted from the sides of the painted sheet, thus allowing them to identify the most efficient

color dyes. When the flashlight was placed on the yellow paint, the top and right edges glowed bright yellow, while the bottom and left edges glowed bright pink. This was due to the fact that the emission from the pink dye at the center overcame the emitted color of the yellow paint (Figure 17a). When the flashlight was placed at the center, all of the edges glowed orange evenly, and far brighter than when placing the flashlight at the corners (Figure 17b). This is because the traveling distance of the light was equal and the re-absorption of the re-emitted light was

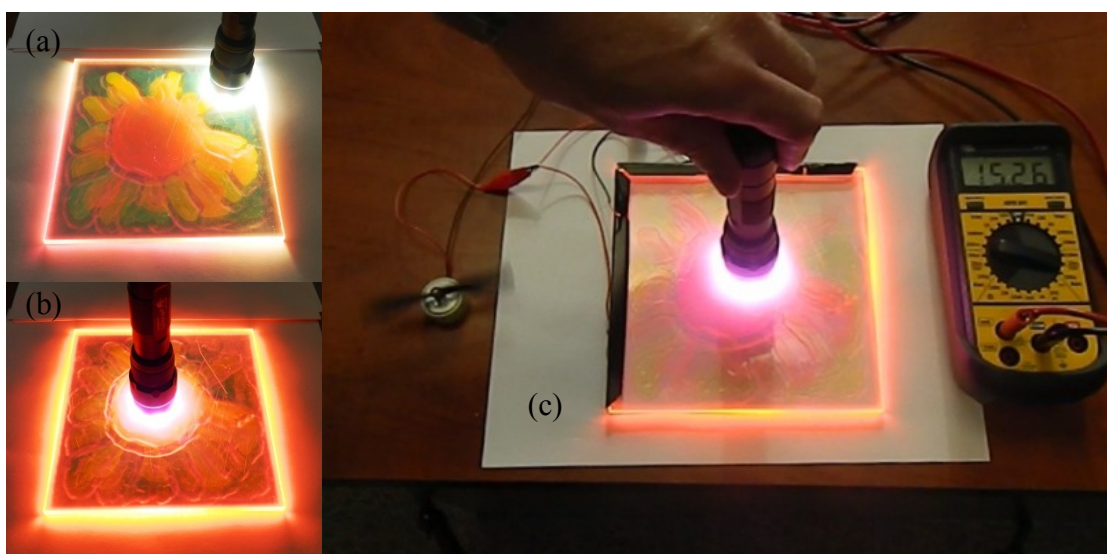


Figure 17 (a) Paintings under flashlight on the top of upper right corner; (b) Paintings under flashlight on the top of center; (c) LSC kit assembly with multimeter and motor.

minimized. The students also learned that the more intense and shorter wavelength light would produce greater power outputs. But most important was that the students thoroughly enjoyed seeing the glow of the paints and determining the results of their paintings' power outputs. They were allowed to take their paintings home, so to spread their knowledge and the experience at Michigan State University to their peer groups and families.

SUMMARY AND FUTURE WORK

This thesis has presented the research, building retrofit projects, and outreach activity that SPARTA has spearheaded. Chapter one has shown the significance of solar PV angular dependency on overall power output: by improving the angular dependency at oblique incident angles, the overall power output can increase as much as 30%, and the design cut-off angle of this property is 70° - 80° . Also, it is important to incorporate the angular dependency of solar PV into computational models for estimating power output in the future. This will yield more accurate modeling results, which will affect the optimal layout design of solar PV arrays, and essentially affect the financial decisions.

Chapter two has summarized three building retrofit projects, which helped MSU move towards a greener campus. The survey on rooftop solar PV installation viability shows that the estimated overall viable roof area is 401700 m^2 , and it subjects to produce 11MW power, which will substitute 17.5% of the current electricity consumption on campus. The study needs to be continued by doing detailed PV arrays layout designs on each building specifically to improve the accuracy of actual power output, financial feasibility, and structural feasibility.

The particular window film study examined in the Kresge Art Center did not show a favorable payback. However, the study was confined to a unique situation where the solar heat only made up for 50% of the total heat transmission and the sole room was widely open to other space, which greatly reduced the energy savings impact of the window film. Therefore, it is recommended that this study to be conducted in a complete building with better controlled space. Nonetheless, the aesthetic and psychological benefits that window film adds to the building are convincing.

The LED retrofit so far is the most effective way to reduce building energy load and is the most financially feasible project (payback time < 3 years). The study at Psychology building

shows that the electricity consumption by light will be reduced by 46.6% with a total lifetime cost saving of \$44,875. The key factor on the financial impact was found to be the operating hours of the light fixtures, and is even more important than the unit price. Once the operating time drops to 12 hours per day, the payback time is almost doubled. Therefore, the LED retrofit will be suitable for places that the lights are constantly on such as hallways and bathrooms, and future efforts should focus on indemnifying those areas for installation.

Chapter three illustrates an in-class activity to educate students about solar energy using luminescent solar concentrators. It is also an interactive and fun experience combined science and art together to teach the students about waveguiding and electrical circuits. In the future, additional color options can be added to the collection, with stronger luminescence allowing the generated energy to power a greater range of electronic devices. In conclusion, SPARTA will continue to carry out research, pilot studies, and outreach activities to promote renewable energy but has already made substantial strides in many of these renewable energy areas.

APPENDICES

APPENDIX I. Survey Summary of MSU Rooftop Solar Installation

Table 6 MSU rooftop solar installation building list

Building Name	Roof Type	Total Viable Area (sq.ft.)	Total Flat Area (sq.ft.)	Total E/W Facing Area (sq.ft.)	Total S Facing Area (sq.ft.)	Electricity of 2014 (MWh)	AIM
DEMONSTRATION HALL	combine	25287	14235	0	11052	253	56.2
FARRALL, A.W., AGRICULTURAL ENGINEERING HALL	combine	36321	30679	0	5642	689	44.5
ENGINEERING RESEARCH - JOLLY RD	combine	7890	6057	0	1833	186	32.5
MUNN, CLARENCE L., ICE ARENA	combine	83202	68009	9116	6077	2487	27.4
KEDZIE HALL	combine	36901	25794	3821	7286	1094	23.6
UNION BUILDING	combine	34667	31016	3651	0	1865	16.6
OLD HORTICULTURE	combine	5569	3954	1615	0	254	15.5
MUSIC BUILDING	combine	13129	10285	2844	0	692	14.9
AUDITORIUM	combine	21949	9381	0	12568	695	13.5
DUFFY "HUGH" DAUGHERTY FOOTBALL AND CLARA BELL SMITH STUDENT ATHLETE ACADEMIC CENTER	combine	113334	27472	85862	0	2205	12.5
ENGINEERING RESEARCH COMPLEX	combine	88589	36608	35587	16394	4024	9.1
BUTTERFIELD HALL	flat	25176	25176	0	0	135	186.5

Table 6 (cont'd)

ANGELL, ROBERT D., UNIVERSITY SERVICES BUILDING	flat	85318	85318	0	0	512	166. 7
MSU SURPLUS STORE & RECYCLING CENTER	flat	71694	71694	0	0	506	141. 7
LINEN SERVICES	flat	35717	35717	0	0	425	84.0
INTRAMURAL RECREATIVE SPORTS EAST	flat	52844	52844	0	0	638	82.8
PAVILION FOR AGRICULTURE AND LIVESTOCK EDUCATION - MAIN BUILDING	flat	165066	16506 6	0	0	2150	76.8
INFRASTRUCTU RE PLANNING AND FACILITIES	flat	60133	60133	0	0	913	65.8
WELLS HALL	flat	55126	55126	0	0	851	64.7
URBAN PLANNING & LANDSCAPE ARCHITECTURE - INSTRUCTIONAL MEDIA CENTER	Flat	17934	17934	0	0	292	61.5
PUBLIC SAFETY	flat	33822	33822	0	0	652	51.8
WHARTON, CLIFTON & DELORES, CENTER FOR PERFORMING ARTS	flat	70067	70067	0	0	1390	50.4
COMMUNICATIO N ARTS & SCIENCES BUILDING	flat	102775	10277 5	0	0	2072	49.6
BRYAN HALL	flat	27821	27821	0	0	580	47.9
PACKAGING	flat	35049	35049	0	0	736	47.6

Table 6 (cont'd)

MSU COLLEGE OF LAW	flat	91484	91484	0	0	1929	47.4
WONDERS HALL	flat	65750	65750	0	0	1420	46.3
MCDONEL HALL	flat	74718	74718	0	0	1621	46.1
EMMONS HALL	flat	25636	25636	0	0	579	44.3
WILSON HALL	flat	85903	85903	0	0	1972	43.6
ARMSTRONG HALL	flat	23504	23504	0	0	599	39.3
HOLDEN HALL	flat	77037	77037	0	0	2093	36.8
HOLMES HALL	flat	95972	95972	0	0	2623	36.6
NATURAL RESOURCES	flat	60749	60749	0	0	1661	36.6
RATHER HALL	flat	24596	24596	0	0	674	36.5
CONRAD HALL	flat	14038	14038	0	0	406	34.6
RADIOLOGY - MAIN BUILDING	flat	32698	32698	0	0	957	34.2
BUSINESS COLLEGE COMPLEX	flat	64509	64509	0	0	1888	34.2
BAILEY HALL	flat	26833	26833	0	0	788	34.1
BESSEY HALL	flat	36612	36612	0	0	1082	33.8
FOOD STORES	flat	71255	71255	0	0	2124	33.5
ERICKSON HALL	flat	44070	44070	0	0	1398	31.5
MANLY MILES BUILDING	flat	20686	20686	0	0	666	31.0
SHAW HALL	flat	61477	61477	0	0	2016	30.5
FEE HALL	flat	77339	77339	0	0	2678	28.9
BAKER HALL	flat	10174	10174	0	0	366	27.8
RHS INFORMATION SERVICES	flat	11520	11520	0	0	417	27.7
HUBBARD HALL	flat	58736	58736	0	0	2421	24.3
BRODY HALL	flat	80671	80671	0	0	3389	23.8
KRESGE ART CENTER	flat	34688	34688	0	0	1458	23.8
OWEN GRADUATE HALL	flat	52978	52978	0	0	2268	23.4

Table 6 (cont'd)

CLINICAL CENTER - OFFICE - LAB. WING	flat	12284	12284	0	0	538	22.8
INTERNATIONAL CENTER	flat	40046	40046	0	0	1996	20.1
JENISON FIELDHOUSE	flat	79850	44591	35259	0	2251	19.8
VETERINARY MEDICAL CENTER	flat	158080	158080	0	0	8342	18.9
NISBET, STEVEN S., BUILDING	flat	13598	13598	0	0	725	18.7
LIFE SCIENCE	flat	56508	56508	0	0	3100	18.2
CLINICAL CENTER - CLINIC	flat	53326	53326	0	0	3109	17.2
AKERS HALL	flat	28490	28490	0	0	1756	16.2
GEOGRAPHY BUILDING	flat	10976	10976	0	0	721	15.2
PSYCHOLOGY BUILDING	flat	15766	15766	0	0	1090	14.5
Executive Development Center	flat	25852	25852	0	0	1890	13.7
OLIN MEMORIAL HEALTH CENTER	flat	11051	11051	0	0	823	13.4
OLDS HALL	flat	6375	6375	0	0	502	12.7
ENGINEERING BUILDING	flat	105846	105846	0	0	9625	11.0
CASE HALL	flat	30925	30925	0	0	2859	10.8
LIBRARY	flat	60999	60999	0	0	6703	9.1
AG HALL (JUSTIN S. MORRILL HALL OF AGRICULTURE)	flat	6000	6000	0	0	709	8.5
CLINICAL CENTER - ANIMAL QUARTERS WING	flat	13742	13742	0	0	1714	8.0
SNYDER AND PHILLIPS HALL	flat	19477	19477	0	0	2460	7.9

Table 6 (cont'd)

FOOD SAFETY AND TOXICOLOGY BUILDING	flat	24230	24230	0	0	3097	7.8
HANNAH, JOHN A., ADMINISTRATION BUILDING	flat	26535	26535	0	0	3394	7.8
KELLOGG CENTER	flat	30598	30598	0	0	4959	6.2
TROUT, G. MALCOLM, FOOD SCIENCE AND HUMAN NUTRITION BUILDING	flat	20913	20913	0	0	3756	5.6
CYCLOTRON	flat	129018	129018	0	0	25207	5.1
SPARTAN STADIUM - OFFICE TOWER (SPARTAN WAY)	flat	21418	21418	0	0	4443	4.8
PLANT BIOLOGY LABORATORIES	flat	41149	41149	0	0	9064	4.5
PLANT & SOIL SCIENCES BUILDING	flat	52152	52152	0	0	12197	4.3
BIOCHEMISTRY	flat	21525	21525	0	0	5563	3.9
DIAGNOSTIC CENTER FOR POPULATION AND ANIMAL HEALTH	flat	35934	35934	0	0	9435	3.8
DAIRY CATTLE TEACHING & RESEARCH CENTER - MAIN BARN	sloped	24471	0	13420	11051	not available	not available
COMPOSTING FACILITY SOUTH CAMPUS	sloped	18857	0	0	18857	not available	not available

Table 6 (cont'd)

Equine Performance Center	sloped	18399	0	1921	16478	not available	not available
UNIVERSITY FARMS SERVICE CENTER - 4-H BUILDING	sloped	14554	0	14554	0	not available	not available
CANDLEWOOD SUITES	sloped	14330	0	7165	7165	not available	not available
DAIRY CATTLE TEACHING & RESEARCH CENTER - SOUTH HAY BARN	sloped	13420	0	13420	0	not available	not available
UNIVERSITY FARMS SERVICE CENTER - NORTH MORTON	sloped	10701	0	10701	0	not available	not available
UFSC Storage Barn	sloped	10496	0	10496	0	not available	not available
UNIVERSITY FARMS SERVICE CENTER - MAINTENANCE BUILDING	sloped	10318	0	10318	0	not available	not available
UNIVERSITY FARMS SERVICE CENTER - COMMUNITY STORAGE	sloped	9442	0	9442	0	not available	not available
VETERINARY MEDICAL CENTER - MATILDA R. WILSON, PEGASUS CRITICAL CARE CENTER	sloped	9061	0	5222	3839	not available	not available
CROP SCIENCE - STORAGE BUILDING	sloped	7552	0	0	7552	not available	not available

Table 6 (cont'd)

AMTRAK STATION	sloped	7166	0	0	7166	not available	not available
ENTOMOLOGY FIELD & RESEARCH CENTER - MAIN BUILDING	sloped	67115	0	67115	0	11	5336.3
BEEF CATTLE RESEARCH CENTER - MAIN BUILDING	sloped	29087	0	4756	24331	93	303.6
SHEEP TEACHING & RESEARCH CENTER	sloped	7785	0	3525	4260	40	179.2
PAVILION FOR AGRICULTURE AND LIVESTOCK EDUCATION - HORSE BARN	sloped	13681	0	0	13681	83	165.1
BOTANY FIELD LABORATORY - LABORATORY BUILDING	sloped	9173	0	9173	0	51	154.0
Beef and Cattle Research Barn	sloped	7816	0	0	7816	93	83.6
SWINE TEACHING & RESEARCH CENTER	sloped	17202	0	7405	9797	240	66.9
JOHN & MARNIE DEMMER SHOOTING SPORTS EDUCATION AND TRAINING CENTER	sloped	17228	0	10831	6397	245	63.6
LINTON, ROBERT S., HALL	sloped	15759	0	6644	1337	285	51.8

Table 6 (cont'd)

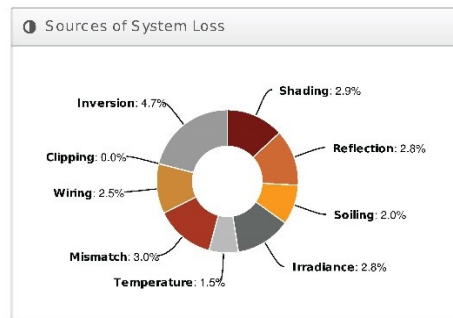
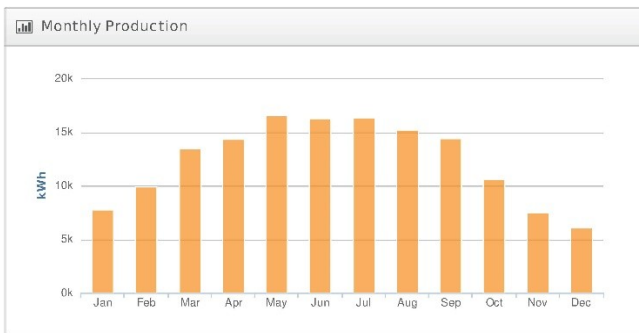
HANCOCK TURFGRASS FIELD LABORATORY	sloped	3000	0	0	3000	64	46.7
SPARTAN CHILD DEVELOPMENT CENTER	sloped	9632	0	4816	4816	279	31.9
ENGINEERING RESEARCH JOLLY ROAD - CONCRETE LABORATORY	sloped	9721	0	7356	2365	288	29.9
CROP SCIENCE - FIELD LABORATORY	sloped	21353	0	16015	5338	685	27.6
BERKEY HALL	sloped	15246	0	7623	7623	738	19.1

APPENDIX II. HelioScope Report of Wells Hall

Design 1 Wells Detailed, Wells Hall, East Lansing, MI

Report	
Project Name	Wells Detailed
Project Address	Wells Hall, East Lansing, MI
Prepared By	Yunhua Ding msusparta@gmail.com
	

System Metrics	
Design	Design 1
DC Nameplate	120.1 kW
AC Nameplate	105.0 kW Load Ratio: 1.14
Production	148.5 MWh
Performance Ratio	79.7%
kWh/kWp	1,236.7
Weather Dataset	TMY, LANSING CAPITAL CITY ARPT, NSRDB (tmy3, I)
Simulator Version	87 (6bda50cc2c-87592d2f8d-23f64ac7e2-1c64cc7ad4)



Annual Production			
	Description	Output	% Delta
Irradiance (kWh/m ²)	Annual Global Horizontal Irradiance	1,367.6	
	POA Irradiance	1,550.7	13.4%
	Shaded Irradiance	1,505.5	-2.9%
	Irradiance after Reflection	1,462.8	-2.8%
	Irradiance after Soiling	1,433.6	-2.0%
Total Collector Irradiance		1,433.6	0.0%
Energy (kWh)	Nameplate	172,103.3	
	Output at Irradiance Levels	167,270.6	-2.8%
	Output at Cell Temperature Derate	164,787.3	-1.5%
	Output After Mismatch	159,840.7	-3.0%
	Optimal DC Output	155,829.2	-2.5%
	Constrained DC Output	155,817.6	0.0%
	AC Output	148,548.4	-4.7%
Energy to Grid		148,548.4	0.0%
Temperature Metrics			
Avg. Operating Ambient Temp		12.0 °C	
Avg. Operating Cell Temp		18.8 °C	
Simulation Metrics			
		Operating Hours	4675
		Solved Hours	4675

Condition Set			
Description	Condition Set 1		
Weather Dataset	TMY, LANSING CAPITAL CITY ARPT, NSRDB (tmy3, I)		
Solar Angle Location	Meteo Lat/Lng		
Transposition Model	Perez Model		
Temperature Model	Sandia Model		
Temperature Model Parameters	Rack Type	a	b
	Fixed Tilt	-3.56	-0.075
Temperature Model Parameters	Flush Mount	-2.81	-0.0455
			Temperature Delta
Soiling (%)	J	F	M
	A	M	J
	J	A	S
	O	N	D
	2	2	2
	2	2	2
	2	2	2
	2	2	2
	2	2	2
	2	2	2
	2	2	2
	2	2	2
Irradiation Variance			
5%			
Cell Temperature Spread			
4° C			
Module Binning Range			
-2.5% to 2.5%			
AC Conductor Derate			
0.00%			
Module Characterizations		Characterization	
Module		STP210S-18/Ub-1 (Suntech)	
		Default Characterization, PAN	
Component Characterizations		Characterization	
Device		SINVERT 100 M-3DC (Siemens)	
		Default Characterization	

Figure 18 Helioscope report capture of Wells Hall

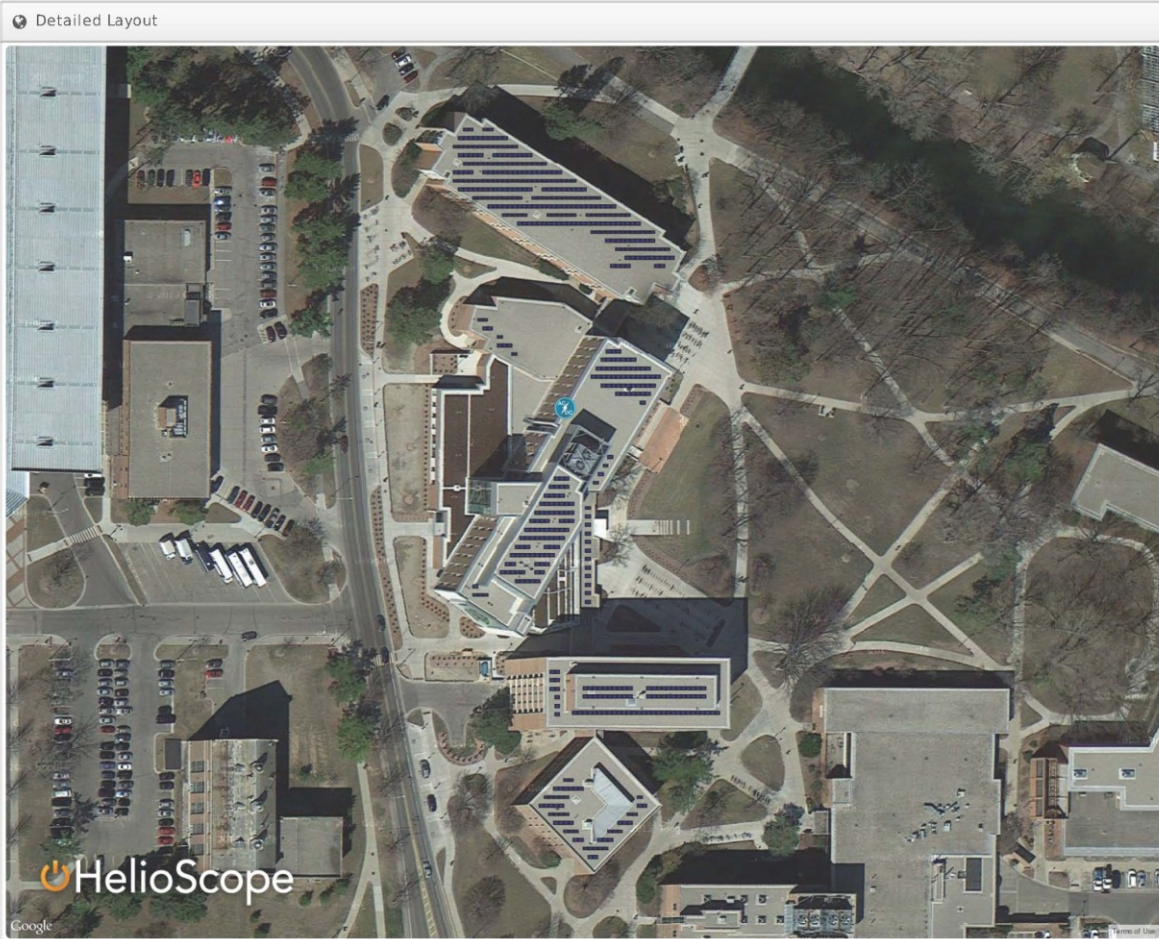
Figure 18 (cont'd)

Components		
Component	Name	Count
Inverter	SINVERT 100 M-3DC (Siemens)	1 (105.0 kW)
Combiners	None	4
Home Runs	10 AWG (Copper)	3 (506.8 ft)
Strings	10 AWG (Copper)	26 (6,618.0 ft)
Module	STP210S-18/Ub-1 (Suntech)	52

Wiring Zones			
Description	Combiner Poles	String Size	Stringing Strategy
Wiring Zone	12	22	Along Racking

Field Segments								
Description	Racking	Orientation	Tilt	Azimuth	Intrarow Spacing	Frame Size	Frames	Modules
Field Segment 1	Fixed Tilt	Horizontal (Landscape)	33°	180°	5.5 ft	1x1	54	54
Field Segment 2	Fixed Tilt	Horizontal (Landscape)	33°	180°	5.5 ft	1x1	83	83
Field Segment 3	Fixed Tilt	Horizontal (Landscape)	33°	180°	5.5 ft	1x1	4	4
Field Segment 4	Fixed Tilt	Horizontal (Landscape)	33°	180°	5.5 ft	1x1	271	271
Field Segment 5	Fixed Tilt	Horizontal (Landscape)	33°	180°	5.5 ft	1x1	9	9
Field Segment 6	Fixed Tilt	Horizontal (Landscape)	33°	180°	5.5 ft	1x1		
Field Segment 7	Fixed Tilt	Horizontal (Landscape)	33°	180°	5.5 ft	1x1	12	12
Field Segment 8	Fixed Tilt	Horizontal (Landscape)	33°	180°	5.5 ft	1x1	4	4
Field Segment 9	Fixed Tilt	Horizontal (Landscape)	33°	180°	5.5 ft	1x1	44	44
Field Segment 10	Fixed Tilt	Horizontal (Landscape)	33°	180°	5.5 ft	1x1	9	9
Field Segment 11	Fixed Tilt	Horizontal (Landscape)	33°	180°	5.5 ft	1x1	30	30
Field Segment 12	Fixed Tilt	Horizontal (Landscape)	33°	180°	5.5 ft	1x1		
Field Segment 13	Fixed Tilt	Horizontal (Landscape)	33°	180°	5.5 ft	1x1	52	52

Figure 18 (cont'd)



BIBLIOGRAPHY

BIBLIOGRAPHY

1. *About Our Plan*. About [cited 2014 Nov 1]; Available from: <http://www.energytransition.msu.edu/about.html>.
2. *Measuring Progress*. Energy Transition Plan 2014 [cited 2014 Nov 1]; Available from: <http://www.energytransition.msu.edu/progress.html>.
3. Oliver, M. and T. Jackson, *Energy and economic evaluation of building-integrated photovoltaics*. Energy, 2001. **26**(4): p. 431-439.
4. Hammond, G.P., et al., *Whole systems appraisal of a UK Building Integrated Photovoltaic (BIPV) system: Energy, environmental, and economic evaluations*. Energy Policy, 2012. **40**(0): p. 219-230.
5. Pagliaro, M., R. Ciriminna, and G. Palmisano, *BIPV: merging the photovoltaic with the construction industry*. Progress in Photovoltaics: Research and Applications, 2010. **18**(1): p. 61-72.
6. Chang, T.P., *The Sun's apparent position and the optimal tilt angle of a solar collector in the northern hemisphere*. Solar Energy, 2009. **83**(8): p. 1274-1284.
7. Yadav, A.K. and S.S. Chandel, *Tilt angle optimization to maximize incident solar radiation: A review*. Renewable and Sustainable Energy Reviews, 2013. **23**(0): p. 503-513.
8. der Wiel, B.v., et al., *Market Readiness of Organic Photovoltaics for Building Integration*. MRS Online Proceedings Library, 2014. **1639**: p. mrsf13-1639-y10-03.
9. Dennler, G., et al., *Angle dependence of external and internal quantum efficiencies in bulk-heterojunction organic solar cells*. Journal of Applied Physics, 2007. **102**(5): p. 054516.
10. Lee, S., et al., *Effect of incidence angle and polarization on the optimized layer structure of organic solar cells*. Solar Energy Materials and Solar Cells, 2013. **118**(0): p. 9-17.
11. Persson, N.-K., H. Arwin, and O. Inganäs, *Optical optimization of polyfluorene-fullerene blend photodiodes*. Journal of Applied Physics, 2005. **97**(3): p. 034503.
12. Cheyns, D., et al., *The angular response of ultrathin film organic solar cells*. Applied Physics Letters, 2008. **92**(24): p. 243310.
13. Pettersson, L.A.A., L.S. Roman, and O. Inganäs, *Quantum efficiency of exciton-to-charge generation in organic photovoltaic devices*. Journal of Applied Physics, 2001. **89**(10): p. 5564-5569.

14. Chen, C.-C., et al., *Visibly Transparent Polymer Solar Cells Produced by Solution Processing*. ACS Nano, 2012. **6**(8): p. 7185-7190.
15. Lunt, R.R. and V. Bulovic, *Transparent, near-infrared organic photovoltaic solar cells for window and energy-scavenging applications*. Applied Physics Letters, 2011. **98**(11): p. 113305.
16. Song, J.-H., et al., *Power output analysis of transparent thin-film module in building integrated photovoltaic system (BIPV)*. Energy and Buildings, 2008. **40**(11): p. 2067-2075.
17. Young, M., et al., *Angle dependence of transparent photovoltaics in conventional and optically inverted configurations*. Applied Physics Letters, 2013. **103**(13): p. 133304.
18. Yan, X., et al., *Enhanced Omnidirectional Photovoltaic Performance of Solar Cells Using Multiple-Discrete-Layer Tailored-and Low-Refractive Index Anti-Reflection Coatings*. Advanced Functional Materials, 2013. **23**(5): p. 583-590.
19. Kuo, S.-Y., et al., *Dandelion-shaped nanostructures for enhancing omnidirectional photovoltaic performance*. Nanoscale, 2013. **5**(10): p. 4270-4276.
20. *Reference Solar Spectral Irradiance: Air Mass 1.5*. Renewable Resource Data Center [cited 2014 Nov 1]; Available from: <http://rredc.nrel.gov/solar/spectra/am1.5>.
21. Hay, J.E., *Calculation of monthly mean solar radiation for horizontal and inclined surfaces*. Solar Energy, 1979. **23**(4): p. 301-307.
22. Wilcox, S., *National Solar Radiation Database 1991-2010 Update User's Manual*. 2012.
23. El-Sebaili, A.A., et al., *Global, direct and diffuse solar radiation on horizontal and tilted surfaces in Jeddah, Saudi Arabia*. Applied Energy, 2010. **87**(2): p. 568-576.
24. *National Renewable Energy Laboratory PVWatts Version 1*. Accessible at: <http://rredc.nrel.gov/solar/calculators/pvwatts/version1/>. Accessed October 4, 2013.
25. Lunt, R.R., et al., *Practical Roadmap and Limits to Nanostructured Photovoltaics*. Advanced Materials, 2011. **23**(48): p. 5712-5727.
26. Shrotriya, V., Li, G., Yao, Y., Moriarty, T., Emery, K. and Yang, Y., *Accurate Measurement and Characterization of Organic Solar Cells*. Adv. Funct. Mater., 2006. **16**: p. 2016–2023.
27. Tang, R. and T. Wu, *Optimal tilt-angles for solar collectors used in China*. Applied Energy, 2004. **79**(3): p. 239-248.
28. Kaldellis, J., K. Kavadias, and D. Zafirakis, *Experimental validation of the optimum photovoltaic panels' tilt angle for remote consumers*. Renewable Energy, 2012. **46**: p. 179-191.

29. *Feasibility Study - Solar Technologies for MSU*. 2012, Black and Veatch.
30. *Renewable Energy and Conservation Technologies*. [Report] [cited 2014 Nov 1]; Available from: <http://energytransition.msu.edu/documents/renewableemergingenergy-final.pdf>.
31. *Projects*. Energy Transition Plan [cited 2014 Nov 1]; Available from: <http://www.energytransition.msu.edu/projects.html#betterbuildingschallenge>.
32. *Incandescents Going Out with a Bang, NEMA Report Finds*. Discover Lighting [cited 2014 Dec 4]; Available from: http://www.ies.org/LDA/E-newsletter/2012/April/newswire/2012_04-nema.cfm.
33. *The Lighting Handbook: Reference and Application*, ed. D.L. Dilaura, et al. 2011, New York, NY: Illuminating Engineering Society of North America.
34. *New Window Technology Saves Energy and the View*. 2013 [cited 2014 Nov 1]; Available from: <http://www.energy.gov/articles/new-window-technology-saves-energy-and-view>.
35. *Benefits of Efficient Windows*. [cited 2014 Nov 1]; Available from: <http://www.efficientwindows.org/benefits.php>.
36. *PV Module Temperature*. Modules and Arrays [cited 2014 Nov 1]; Available from: <http://pveducation.org/pvcdrom/modules/pv-module-temperature>.
37. *MSU Facts*. [cited 2014 Nov 1]; Available from: <https://www.msu.edu/about/thisismsu/facts.html>.
38. *Generating Power*. [cited 2014 Nov 1]; Available from: <http://ipf.msu.edu/green/energy/generating-power.html>.
39. *PVWatts - A Performance Calculator for Grid-Connected PV Systems*. Renewable Resources Data Center [Database] Nov 3, 2014; Available from: <http://rredc.nrel.gov/solar/calculators/pvwatts/version1/>.
40. Arribas, L., et al. *World-wide Overview of Design and Simulation Tools for Hybrid PV Systems*. 2011 [cited 2014 Nov 30]; Available from: http://www.iea-pvps.org/fileadmin/dam/public/report/technical/rep11_01.pdf.
41. Grossman, A., *Renewable Energy and Conservation Measures for Non-residential Buildings*, in *Mechanical Engineering*. 2014, Michigan State University: East Lansing, MI, USA.
42. Kann, S., et al. *Solar Market Insight Report 2014 Q1*. [cited 2014 Nov 3]; Available from: <http://www.seia.org/research-resources/solar-market-insight-report-2014-q1>.

43. *LED Basics*. SSL Basics [cited 2014 Nov 30]; Available from: <http://energy.gov/eere/ssl/led-basics>.
44. Sark, W.G.J.H.M.v., et al., *Luminescent Solar Concentrators - A review of recent results*. Optics Express, 2008. **16**(26): p. 21773-21792.
45. Trupke, T., M.A. Green, and P. Würfel, *Improving solar cell efficiencies by up-conversion of sub-band-gap light*. Journal of Applied Physics, 2002. **92**(7): p. 4117-4122.
46. Trupke, T., M.A. Green, and P. Würfel, *Improving solar cell efficiencies by down-conversion of high-energy photons*. Journal of Applied Physics, 2002. **92**(3): p. 1668-1674.
47. Tsoi, S., *Structured luminescent solar energy concentrators : a new route towards inexpensive photovoltaic energy*, in *Department of Chemical Engineering and Chemistry*. 2012, Technische Universiteit Eindhoven: Eindhoven, Netherland. p. 160.